1

Working group report: QCD

Conveners: J. M. Campbell, K. Hatakeyama, J. Huston, F. Petriello

J. Andersen, L. Barzè, T. Becher, A. Blondel, G. Bodwin, R. Boughezal, E. Braaten, M. Chiesa, G. Dissertori, S. Dittmaier, G. Ferrera, S. Forte, N. Glover, T. Hapola, A. Huss, X.Garcia i Tormo, M. Grazzini, S. Höche, P. Janot, T. Kasprzik, M. Klein, U. Klein, D. Kosower, Y. Li, X. Liu, K. Mishra, G. Montagna, M. Moretti, O. Nicrosini, F. Piccinini, V. Radescu, L. Reina, J. Rojo, J. Russ, J. Smillie, I. W. Stewart, F. J. Tackmann, F. Tramontano, J. R. Walsh, S. Zuberi

July 28, 2013

1.1 Introduction

A detailed understanding of quantum chromodynamics (QCD) phenomenology, both perturbative and non-perturbative, is crucial for a detailed understanding of physics at hadron-hadron, lepton-hadron, and lepton-lepton colliders. The QCD sub-group is somewhat different from most of the other sub-groups in the Snowmass workshop in that the emphasis is not on observables per se, but on the tools needed to understand the observables, in physics processes at all of the colliders mentioned above. There has been a great deal of progress in the last 5-10 years on QCD-related tools for calculation, simulation and analysis, at a level that would have been considered unlikely at best, if predicted at the time of the previous Snowmass workshop. Thus, it is our difficult task to summarize the level of the tools that exist now, to perform this extrapolation into the medium and long-term future, and to present a priority list as to the direction that the development of these tools should take. Most of our efforts concentrate on proton-proton colliders, at 14 TeV as planned for the next run of the LHC, and for 33 and 100 TeV, possible energies of the colliders that will be necessary to carry on the physics program started at 14 TeV. We also examine QCD predictions and measurements at lepton-lepton and lepton-hadron colliders, and in particular their ability to improve our knowledge of $\alpha_s(m_Z)$ (both) and our knowledge of PDFs (lepton-hadron colliders). Since the current world average of strong coupling measurements is dominated by the determinations made using lattice gauge theory we also explore possible improvements to our knowledge of $\alpha_s(m_Z)$ from such extractions.

It is useful to recall the basic structure of a parton-level cross section computed in perturbative QCD. The cross section can be written schematically as,

$$\sigma = \sum_{a,b} \int_0^1 \mathrm{d}x_1\, f_{a/A}(x_1,\mu_F^2) \int_0^1 \mathrm{d}x_2\, f_{b/B}(x_2,\mu_F^2) \Bigg\{ \int \mathrm{d}\hat{\sigma}_{ab}^{LO}\left(\alpha_s\right)\, \Theta_{\rm obs}^{(m)} + \alpha_s(\mu_R^2) \left[\int \left(\mathrm{d}\hat{\sigma}_{ab}^{V}\left(\alpha_s,\mu_R^2\right) + \mathrm{d}\hat{\sigma}_{ab}^{C}\left(\alpha_s,\mu_F^2\right)\right)\, \Theta_{\rm obs}^{(m)} + \int \mathrm{d}\hat{\sigma}_{ab}^{R}(\alpha_s)\, \Theta_{\rm obs}^{(m+1)} \right] \Bigg\} + \ldots \tag{1.1}$$

where we have sketched the terms that contribute up to the next-to-leading order (NLO) level in QCD. The first ingredients in the perturbative description are the parton distribution functions (pdfs), defined for a given species of parton a, b inside incoming hadrons A, B. The pdfs are functions of the parton momentum fractions x_1, x_2 and the factorisation scale μ_F. The leading order prediction depends on the hard matrix

elements, contained in the factor $\mathrm{d}\hat{\sigma}_{ab}^{LO}$, which in turn depend on the value of the strong coupling, α_s, for strongly-interacting final states. In this equation the quantity α_s is a shorthand notation since it must be evaluated at the renormalization scale μ_R, $\alpha_s \equiv \alpha_s(\mu_R^2)$. Finally, the predicted cross section depends on the cuts that are applied to the m-parton configuration in order to define a suitable observable, $\Theta_{\mathrm{obs}}^{(m)}$. In the case of cross sections for multi-jet processes this factor accounts for the jet definition that is required for infrared safety. At NLO there are further contributions, as indicated on the second line of the equation. The virtual diagrams contain an explicit dependence on the renormalization scale, $\mathrm{d}\hat{\sigma}_{ab}^{V}\left(\alpha_s, \mu_R^2\right)$ while the collinear counterterms that are necessary in order to provide an order-by-order definition of the pdfs introduce explicit factorization scale dependence, $\mathrm{d}\hat{\sigma}_{ab}^{C}\left(\alpha_s, \mu_F^2\right)$. The effects of real radiation, $\mathrm{d}\hat{\sigma}_{ab}^{R}(\alpha_s)$ now include a cut on the $(m+1)$-parton configuration. They may therefore be sensitive to kinematic effects that are not present in the m-parton case, for instance the effect of jet vetoes in electroweak processes. At next-to-next-to-leading order (NNLO) we would include terms in equation 1.1 that have an explicit factor of $\alpha_s(\mu_R^2)$ in addition to those present at leading order. In outline the extension is clear, with the introduction of configurations that contain m, $m+1$ and $m+2$ parton. As a result NNLO calculations may be even more sensitive to kinematic effects that are only approximately modelled, if at all, in lower orders. However the interplay between soft and collinear divergences in each of these contributions greatly complicates the calculation of NNLO effects.

From this guiding equation it is clear that detailed QCD predictions require knowledge of:

- parton distribution functions (PDFs) and their uncertainties
- $\alpha_s(m_Z)$ and its uncertainty
- higher order corrections to cross sections
- the impacts of restrictions in phase space, such as jet vetoes

Measurements at 14 TeV and higher will access a wide kinematic range, where PDF uncertainties and the impact of higher order corrections may be large. At scales large compared to the W mass, electroweak (EWK) corrections can be as important as those from higher order QCD; mixed QCD-EWK corrections also gain in importance. Higher energies also imply higher luminosities, which require the ability to isolate the physics of interest from the background of multiple interactions accompanying the higher luminosities. Much of the physics of interest will still involve the production of leptons, jets, etc at relatively low scales. Obtaining theoretical predictions in the presence of strict kinematic cuts, especially those involving high transverse momenta, masses, etc, can result in the creation of large logarithms of ratios of scales involved in the processes. All of these effects mean that, as the center-of-mass energy increases, both the perturbative and non-perturbative environments may make precision measurements of such objects more difficult.

In this contribution, we cannot hope for a comprehensive treatment of all of the above, but will try to summarize the most important aspects of QCD for future colliders.

1.2 Parton density functions

Parton distributions are an essential ingredient of present and future phenomenology at hadron colliders [1, 2, 3]. They are one of the dominant theoretical uncertainties for the characterization of the newly discovered Higgs-like boson at the LHC, they substantially affect the reach of searches for new physics at high final state masses and they limit the accuracy to which precision electroweak observables, like the W boson mass or the effective lepton mixing angle, can be extracted from LHC data [4].

1.2.1 Current knowledge and uncertainties

The determination of the parton distribution functions of the proton from a wide variety of experimental data has been the subject of intense activity in the last years. Various collaborations provide regular updates of their PDF sets. The latest releases from each group are ABM11 [5], CT10 [6], HERAPDF1.5 [7, 8], MSTW08 [9] and NNPDF2.3 [10]. A recent benchmark comparison of the most updated NNLO PDF sets was performed in Ref. [11], where similarities and differences between these five PDF sets above were discussed, and where W, Z and jet production data was used to quantify the level of agreement of the various PDF sets with the Tevatron and LHC measurements.

A snapshot of the comparisons between recent NNLO PDFs at the level of parton luminosities and cross section can be seen in Fig. 1-1, where we compare the gluon-gluon PDF luminosities between the five sets. We also show the predictions for Higgs production cross section in the gluon-fusion channel and in WH associated production.[1] Results have been computed using the settings discussed in Ref. [11].

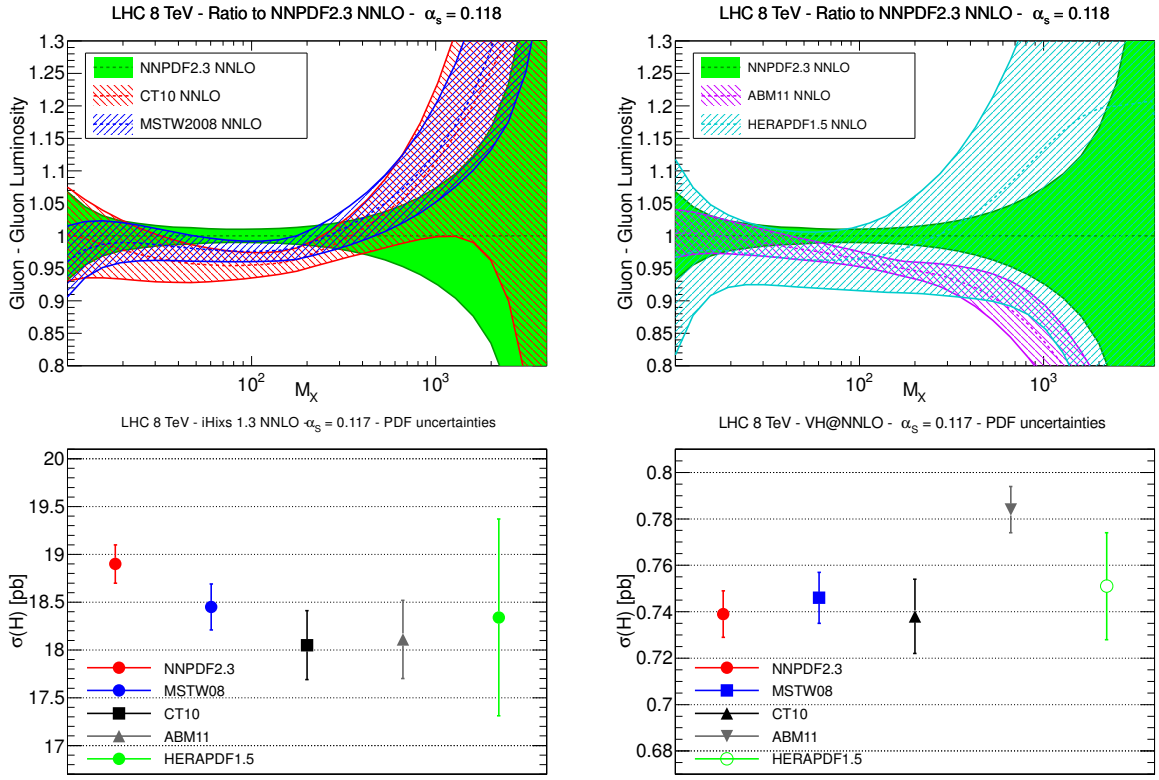

Figure 1-1. *Upper plots: Comparison of the gluon-gluon luminosity at the LHC 8 TeV as a function of the final state mass M_X between the ABM11, CT10, HERAPDF1.5, MSTW and NNPDF2.3 NNLO PDF sets. Lower plots: predictions for the Higgs production cross sections at LHC 8 TeV for the same PDF sets, in the gluon-fusion channel (left plot) and in the WH channel (right plot).*

[1] An extensive set of comparison plots for PDFs, parton luminosities, LHC total cross sections and differential distributions at NLO and NNLO and for different values of $\alpha_s(M_Z)$ can be found in
. `https://nnpdf.hepforge.org/html/pdfbench/catalog/`

As compared to previous comparisons, one of the main conclusions of the benchmark study [11] was that the agreement between the three global PDF sets, CT, MSTW and NNPDF has improved for most PDFs and ranges of Bjorken-x. On the other hand, there are still important differences that need to be understood, and that have substantial phenomenological impact. To begin with, the gluon luminosity for the three PDF sets differs maximally for $m_X \sim 125$ GeV, as can be seen from Fig. 1-1, and it would be important to understand the source of these differences to improve the agreement of the three sets for the gluon-induced Higgs production cross sections. In addition, very large PDF uncertainties affect the production of heavy massive particles, in the TeV range, where also central values can be quite different. These large uncertainties at large masses degrade the prospects for eventual characterization of new BSM heavy particles. On top of this, there are theoretical uncertainties due to the choice of heavy quark general-mass variable-flavor-number (GM-VFN) scheme, specific choices in the fitted dataset and methodological differences that still require further understanding to improve the agreement between the various PDF sets.

In the next subsection we discuss what are the prospects to obtain further constraints in PDFs from LHC data.

1.2.2 Parton distributions with QED corrections

Precision predictions for electroweak processes at hadron colliders require not only (N)NLO QCD corrections, but also the consistent inclusion of QED corrections on parton distribiutions and photon-initiated contributions. QED and electroweak corrections for various relevant collider processes have been computed in the last years in processes like inclusive W, Z production, vector boson pair production, $t\bar{t}$ and dijet production among many others. On the other hand, it is also known that a fully consistent treatment of electroweak corrections requires the use of parton distributions that in turn incorporate QED effects as well. QED effects to parton distributions have two main implications: first of all, the standard QCD DGLAP evolution equations are affected by $\mathcal{O}(\alpha)$ corrections and the associated breaking of isospin invariance, and, phenomenologucally more important, the photon PDF needs to the determined from experimental data just as the quark and gluon PDFs.

Until recently, a single PDF set with QED corrections was available, the MRST2004QED set [25], where the photon PDF was determined based on a model assumption. However, now the NNPDF framework has also been extended to provide PDF sets with QED corrections, and NNPDF2.3 QED is already available in the NNPDF `HepForge` website.[2] NNPDF2.3 QED avoids any model assumption on the photon PDF and derives $\gamma(x, Q^2)$ and its associated uncertainties from a global fit to DIS and LHC data, where in the latter case neutral current and charged current vector boson production data provide stringent constraints on the shape and normalization of $\gamma(x, Q^2)$.[3]

Electroweak corrections to parton distribution functions have important phenomenological implications, in particular for the electroweak production of high invariant mass final states. These include the measurement of the W mass, searches for W' and Z' resonances in the tails of the W and Z distributions and vector boson pair production among many others. The main effect is that the substantial uncertainties on the large-x photon PDF (that stem from the lack of available experimental constraints) translates into very large uncertainties from photon-initiated contributions, that can be as large as a factor 100%.

As an illustration of these phenomenological consequences, in Fig. 1-2 we have computed the predictions of the NNPDF2.3 QED set for WW production at the LHC for various center of mass energies, compared

[2] `https://nnpdf.hepforge.org/html/nnpdf23qed/nnpdf23qed.html`

[3] Preliminary results with the NNPDF2.3 QED set have been presented in Refs. [26, 27], a more detailed paper is in preparation.

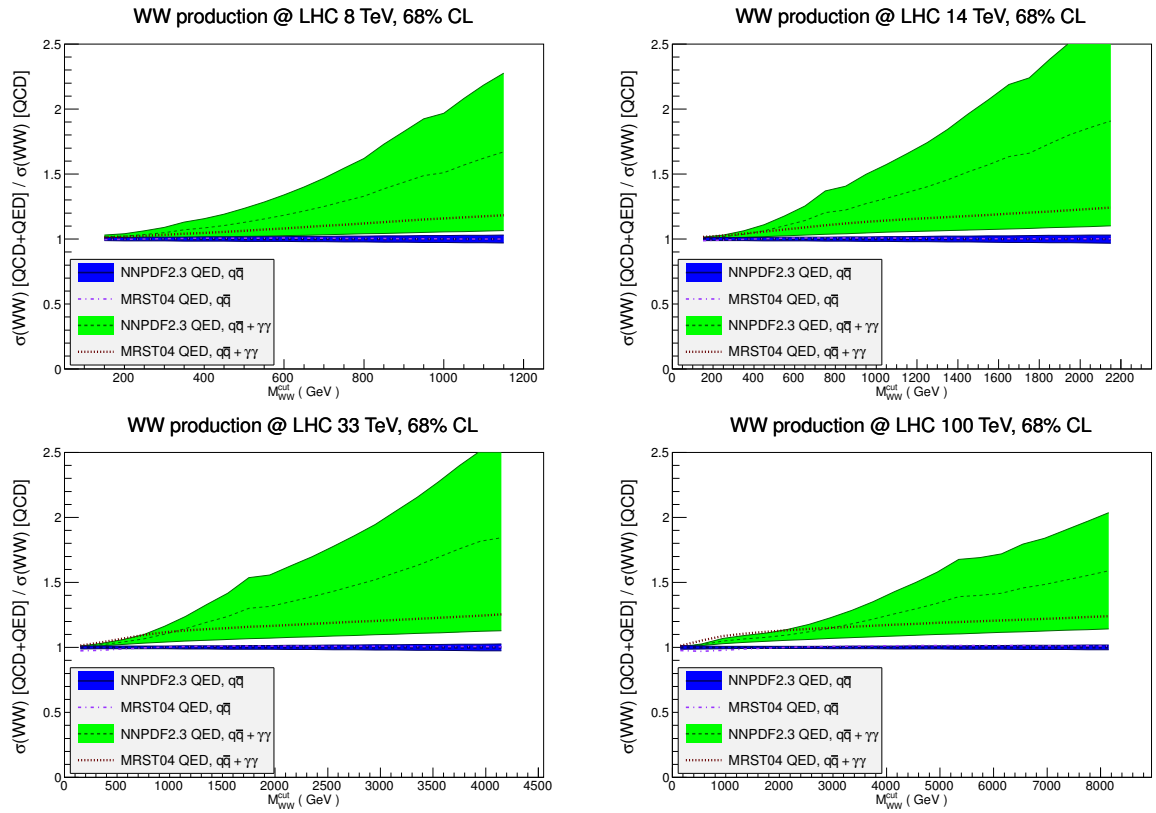

Figure 1-2. *The predictions of the NNPDF2.3 QED set for WW production at the LHC for various center of mass energies, compared with the results of the reference NNPDF2.3 set, as well as with the predictions from MRST2004QED. We show the total cross section as a function of the cut in the $M_{\rm WW}$ invariant mass, for 8, 14, 33 and 100 TeV energies. See text for more details.*

with the results of the reference NNPDF2.3 set, as well as with the predictions from MRST2004QED. The computation has done at leading order in the electroweak coupling but including photon-initiated diagrams, using the same settings as in Ref. [28]. We show the total cross section as a function of the cut in the $M_{\rm WW}$ invariant mass, for 8, 14, 33 and 100 TeV energies.[4] Is clear that the QED-induced theoretical uncertainties are substantial and that do degrade the constraining power of BSM searches in this channel, for instance heavy resonances that decay in WW pairs, and that these effects are more severe the higher the cut in the invariant mass of the WW pair. Of course, as the energy is increased, for a given value of M_{WW} the PDF uncertainties decrease, but they are still very substantial at the highest available masses in each case, a factor 2 at least.

In summary, the development of parton distributions with QED corrections is an important ingredient of fully consistent theoretical predictions of hadron collider processes that include both higher order corrections in the QCD and EW couplings. On the other hand, the same analysis reveal the urgent need for more experimental data to constrain the photon PDF $\gamma(x, Q^2)$, and thus to reduce the currently large QED-induced uncertainties that affect high mass electroweak production at the LHC.

[4] We thank T. Kasprick for providing us with these results.

1.2.3 PDF constraints from future LHC data

The excellent performance of the Large Hadron Collider is substantially increasing the range of processes that can be used to constrain PDFs in a global analysis. Let's begin with the traditional processes at hadron colliders that have been used for PDF constraints, namely inclusive jets and W, Z production. Inclusive jet and dijet data are now available up to the TeV region from ATLAS and CMS [12, 13], and provide important constrains on the poorly known large-x quarks and gluons. In addition, ATLAS has presented the measurement the ratio of inclusive jet cross sections between 2.76 TeV and 7 TeV [14]. Such ratios between different center of mass energies [15] increase the PDF sensitivity of data taken at a single energy, since on the one hand many experimental uncertainties cancel in a dedicated measurement of a cross section ratio, and on the other hand several theory systematics, like scale variations, cancel as well. In the x-range currently dominated by HERA data ($x < 0.1$ for quarks and $x < 0.05$ for gluons)), and to a lesser extent by fixed-target DIS experiments, it will be difficult for collider measurements to match the precision (theoretical and experimental) achieved at HERA. However, the HERA data provides little constraint in the high mass search regions (for BSM), and it's here where collider measurements at high luminosity, at 14 TeV and at higher energies, can greatly contribute to improvements in the PDF uncertainties for both quarks and gluons. In this respect, recent progress towards the full NNLO QCD corrections for inclusive and dijet production [16] should make it feasible to achieve a few per-cent theoretical accuracy (scale dependence) on these observables by the time of the 13 TeV data taking. Although improving, it may be difficult for the expected experimental precision to match the expected theoretical precision.

The precision measurements of W and Z boson production at hadron colliders provide important information on quark flavor separation, and on top allow to reduce systematic uncertainties of important observables like the W boson mass [4]. While the Z rapidity distribution and the W lepton asymmetry from the Tevatron and the LHC have been by now available for some time, recently the range of available processes has been extended by the measurement of the off-peak neutral current Drell-Yan process by ATLAS, CMS and LHCb. Such measurements provide useful information on the large-x quarks and antiquarks (for high mass) and in the small-x gluon and possible departures from lineal DGLAP evolution, in the case of low mass DY, where particularly striking signatures ave been predicted for the LHCb kinematics. In this respect, future measurements at higher energies will benefit on the one hand an increased coverage in the dilepton invariant mass (in the case of neutral current scattering) allowing to probe very large-x antiquarks, which are effected by very large PDF uncertainties, while on the other hand the measurements in the peak region will benefit from reduced systematics and by negligible statistical uncertainties. To date, DGLAP evolution appears to be sufficient to describe the LHC data, but runs at higher energies may demonstrate the presence of BFKL-like effects.

On top of the traditional processes discussed above, many new collider observables have recently become available for the first time for their use in PDF fits. The recent calculation of the full NNLO top quark production [17] cross section makes possible for the first time to include top quark data into a NNLO analysis to constrain the large-x gluon PDF [18]. This is an important result since top production is currently the only hadronic observable which is both directly sensitive to the gluon and can be included in a NNLO global fit without any approximation. In turn, the more accurate gluon PDF will translate into an improvement of the theory predictions for various high-mass BSM processes driven by the gluon luminosity.

Future precision measurements of differential distributions in top quark pair production will allow more precision constraints on the gluon distribution and an ability to enlarge the range of Bjorken-x where the gluon PDF is being probed, especially once the NNLO calculation of [17] is extended to the fully differential case. In addition to top quark data, the use of LHC isolated photon data and photon+jet data has also been advocated in order to pin down the gluon PDF [21, 22], though this process is affect by missing higher order and non perturbative uncertainties.

Turning to the constraints on the quark sector, the production of W and Z bosons in association with jets, for high p_T values of the electroweak boson, is a clean probe at the LHC of both quark flavor separation and of the gluon PDF [23]. In particular, ratios of W and Z distributions at large p_T provide constrains on quarks and antiquarks while benefiting from substantial cancellations of experimental and theory uncertainties. This is a good example of a process currently limited by statistics, and that with future LHC data will benefit of a much increased constraining power. Another important source of information is on the quark PDFs is W production in association with charm, directly sensitive to the strange PDF [24], the worst known of all light quark flavors. Preliminary results for this important process has been recently measured by both ATLAS and CMS. Interestingly, the two measurements seem to pull in different directions for the strange PDF, with CMS showing good agreement with the strangeness suppression of global PDF fits derived from the neutrino DIS charm production data, while ATLAS prefers a symmetric strange sea, similar as previously derived from their inclusive W and Z data. Including all these datasets into the global PDF fits would then be crucial to determine the optimal strange PDF which accounts for all experimental constraints.

Putting everything together, is clear that the LHC will provide in the next years a plethora of new measurements that will be used to improve our knowledge of parton distributions. Quantitative projections in this respect are difficult since precision measurements, like those used in PDF analysis, are dominated by systematics, which are notoriously difficult to predict. In addition, correcting for pile-up in the high-luminosity phase of the LHC might render even more complicated such analysis. But all in all, there are good prospects that in the next years PDFs will be determined with increasingly better accuracy, in turn improving the theory predictions for Higgs boson characterization and New Physics searches.

1.2.4 Luminosities and uncertainties for 14, 33 and 100 TeV

As discussed above, in order to assess similarities and differences between PDF sets, it is useful to compare parton luminosities for different channels as a function of the final state mass M_X of the produced system, for different values of the hadronic collider energy. In the following we will redo the comparisons presented in Ref. [11], but this time for higher energy incarnations of the LHC, at 14 TeV, 33 TeV and 100 TeV. This comparison is shown in Fig. 1-3, where we compare the quark-quark, quark-antiquark and gluon-gluon luminosities between the most updated CT, MSTW and NNPDF NNLO PDF sets at these three center of mass energies.

While in general we observe reasonable agreement between the three sets, there are also some cases where the agreement is marginal, like for the gluon-gluon luminosity, or even non existing, like the very high mass range for the quark-quark luminosity at 100 TeV. The quark-antiquark luminosities for the 3 PDFs in the W/Z mass range agree well at 14 TeV (and even better at 7 and 8 TeV). For the higher energies (33 and 100 TeV), though, the uncertainties in that mass range rapidly increase as smaller (and less well-determined) quark x-values, not well-constrained by HERA, are probed.

1.2.5 Improvements from LHeC

The Large Hadron Electron Collider (LHeC) is a newly designed ep collider [120]. Based on the intense, high energy hadron beams of the LHC, by adding a new electron beam of typically 60 GeV energy a first TeV energy scale electron-proton and electron-ion collider [5] can be built. As the first application of energy recovery

[5] As HERA never accelerated ions, nor deuterons, the kinematic range in lepton-nucleus (eA) deep inelastic scattering (DIS) is extended with the LHeC by nearly four orders of magnitude in four-momentum squared Q^2 and towards low Bjorken x.

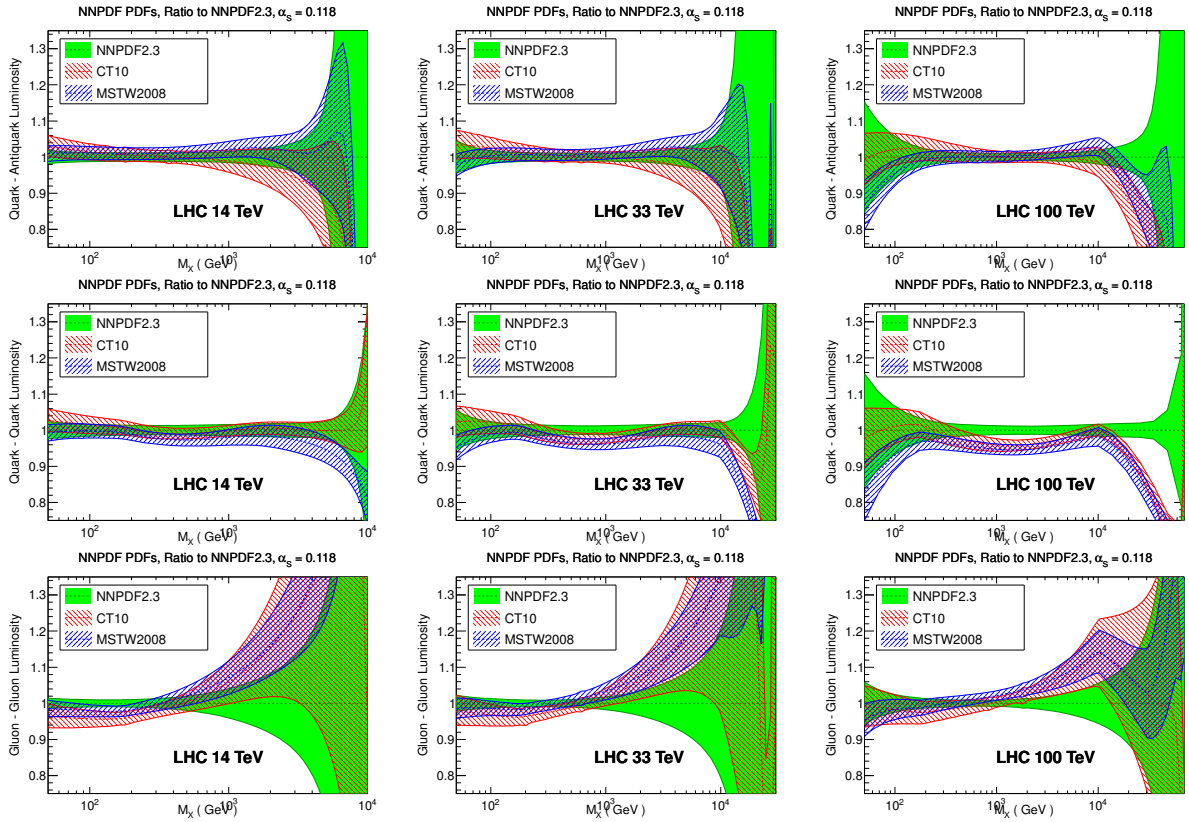

Figure 1-3. *Comparison of the partonic luminosities at 14, 33 and 100 TeV between the CT10, MSTW and NNPDF2.3 NNLO PDF sets. From top to bottom: quark-antiquark luminosity, quark-quark luminosity, and the gluon-gluon luminosity.*

techniques for high energy particle physics, the LHeC is designed to achieve a luminosity in excess [121, 122] of $10^{33}\,\mathrm{cm}^{-2}\mathrm{s}^{-1}$. Very high integrated ep luminosities of several hundreds of fb^{-1}, i.e. around 1000 times more than at HERA, can be collected by operating the new electron machine synchronously with the LHC. Such a huge luminosity enables measurements close to $x = 1$ and the exploitation of the full Q^2 range, up to $Q^2 \simeq 10^6\,\mathrm{GeV}^2$, exceeding the kinematic range of HERA by a factor of 20. The question of gluon saturation at low x can be expected to be settled with precision measurements of the structure functions F_2 and also F_L down to $x \geq 10^{-6}$ [120] while the large x determination of xg is crucial for the LHC Higgs and BSM program [121, 122].

With the LHeC, very precise measurements of charged currents (CC) and the exploitation of Z exchange in neutral currents (NC) become possible, in addition to extending photon exchange NC to extremely low x. The LHeC, combined with HERA to fill in the medium Q^2-larger x region, provides a unique and complete DIS data set. With unprecedented precision there will be for the first time a determination possible of *all* PDFs, $u_v,\ d_v,\ \bar{u},\ \bar{d},\ s,\ \bar{s},\ c,\ b$ and even t, in furthermore a hugely extended kinematic range. To explore this, a full set of NC and CC cross section measurements has been simulated and a QCD fit analysis been applied in order to study the potential for the determination of the parton distribution functions in the proton.

This leads to a determination of the proton but also the neutron and nuclear PDFs in a hugely extended range and with unprecedented diversity, as is described in [120].

As detailed in [120], the strange quark density will be measured for the first time in an accurate way with charm tagging of Ws fusion in CC scattering. Very precise measurements of the charm and the beauty quark density are possible, from Q^2 values below the quark masses squared up to $\sim 10^5\,\mathrm{GeV}^2$, based on the small beam spot size of $\sim 7\,\mu\mathrm{m}^2$ and a high resolution silicon detector of large acceptance. This, for example, will determine the charm mass to a precision of 3 MeV [120], an order of magnitude improved as compared to HERA, and similarly for the bottom mass. Such high precision input will certainly provide a new basis for higher order tests of the treatment of heavy quarks in the Q^2 evolution, which currently is a significant source of uncertainty in the understanding of PDFs and the predictions for LHC.

Monte Carlo data were simulated for NC and CC scattering assuming $e^{\pm}p$ luminosities of $10\,\mathrm{fb}^{-1}$ and a 40 % polarisation. Using the HERAFitter framework [124, 125, 126] with settings based on the HERAPDF NLO QCD fit analysis, a set of PDFs has been generated (and is available on LHAPDF) for estimates of future measurement potentials. An example is the prediction of the $gg \to H$ cross section at the LHC, which will have an uncertainty from PDFs and α_s of only about 0.4 % and thus be sensitive to determinations of M_H via the cross section [122]. Another example is the importance of knowing xg for high mass searches of SUSY particles as has also been recently studied [121, 123].

The procedure used has been adopted from the HERA QCD fit procedure [124] with a mimim Q^2 cut of $3.5\,\mathrm{GeV}^2$ and a starting scale $Q_0^2 = 1.9\ \mathrm{GeV}^2$, chosen to be below the charm mass threshold. The fits have been extended to very low values of x for systematic uncertainty studies, even when at such low x values non-linear effects are expected to appear, eventually altering the evolution laws.

The parameterised PDFs are the valence distributions xu_v and xd_v, the gluon distribution xg, and the $x\bar{U}$ and $x\bar{D}$ distributions, where $x\bar{U} = x\bar{u}$, $x\bar{D} = x\bar{d} + x\bar{s}$. This ansatz is natural to the extent that the NC and CC inclusive cross sections determine the sums of up and down quark distributions, and their antiquark distributions, as the four independent sets of PDFs, which may be transformed to the ones chosen if one assumes $u_v = U - \overline{U}$ and $d_v = D - \overline{D}$, i.e. the equality of anti- and sea quark distributions of given flavour.

The following standard functional form is used to parameterise them

$$xf(x) = Ax^B(1-x)^C(1 + Dx + Ex^2), \tag{1.2}$$

where the normalisation parameters (A_{uv}, A_{dv}, A_g) are constrained by quark counting and momentum sum rules. The parameters $B_{\bar{U}}$ and $B_{\bar{D}}$ are set equal, $B_{\bar{U}} = B_{\bar{D}}$, such that there is a single B parameter for the sea distributions. The strange quark distribution at the starting scale is assumed to be a constant fraction of $\bar{D}$, $x\bar{s} = f_s x\bar{D}$, chosen to be $f_s = 0.5$ such that $\overline{s} = \overline{d}$. In addition, to ensure that $x\bar{u} \to x\bar{d}$ as $x \to 0$, $A_{\bar{U}} = A_{\bar{D}}(1 - f_s)$. The D and E are introduced one by one until no further improvement in χ^2 is found. The best fit resulted in a total of 12 free parameters, specifically fitting $B_g,\ C_g,\ D_g,\ B_{uv},\ C_{uv},\ E_{uv},\ B_{dv},\ C_{dv},\ C_{\overline{U}},\ A_{\overline{D}},\ B_{\overline{D}},\ C_{\overline{D}}$. While the LHeC NC, CC real data, and the inclusion of further information, as of s, c, b and F_L, will certainly lead to quite a different parameterisation, it has been checked that with a more flexible set of 15 parameters very similar results on the PDF uncertainties considered here are obtained.

The PDFs are evolved using DGLAP evolution equations at NLO in the $\overline{MS}$ scheme with the renormalisation and factorisation scales set to Q^2 using standard sets of parameters as for $\alpha_s(M_Z)$. These, as well as the exact treatment of the heavy quark thresholds, have no significant influence on the estimates of the PDF uncertainties. The experimental uncertainties on the PDFs are determined using the $\Delta\chi^2 = 1$ criterion. The LHeC Design Report [120] contains a very detailed presentation of the results of the present analysis for valence and sea quarks with many remarkable features as the determination of the u/d ratio or the measurement of the valence quarks down to low $x \simeq 10^{-4}$.

1.2.5.1 Determination of the Gluon Distribution at the LHeC

The result on the gluon distribution is presented in Fig. 1-4. In the left panel, recent gluon distribution determinations and their uncertainties are shown plotted as a ratio to MSTW08. Below $x \simeq 10^{-3}$ the HERA data have vanishing constraining power due to kinematic range limitations and the gluon is just not determined at low x. At large $x \geq 0.3$ the gluon distribution becomes very small and large variations appear in its determination, differing by orders of magnitude, which is related to uncertainties of jet data, theory uncertainties and the fact that HERA had not enough luminosity to cover the high x region where, moreover, the sensitivity to xg diminishes, as the valence quark evolution is insensitive to it. The larger x situation can be expected to still improve with LHC jet and possibly top and the HERA II data. The right panel shows the experimental uncertainty of xg based on the LHeC, on HERA alone and in various combinations with further data, see the LHeC design report [120]. At small x a few per cent precision becomes possible, compare right with left. Note that the non-LHeC low x uncertainty bands (right) remain narrow below $x \simeq 10^{-3}$ solely as an artefact due to the parameterisation of xg. It is for the LHeC to discover whether xg saturates or not and whether indeed the DGLAP equations need to be replaced by non-linear parton evolution equations such as BFKL. This is important for QCD but as well for super high energy neutrino physics and low x physics at the LHC. In the region of the Higgs data at the LHC, $x \sim 0.02$, the LHeC will pin down the gluon extremely accurately and the $gg \to H$ cross section uncertainties will essentially be removed as has been discussed in [122]. At large values of e.g. $x = 0.6$ the LHeC can be expected to determine xg to $5 - 10\,\%$ precision (inner blue band). This is crucial for when the LHC operates at maximum luminosity and the searches approach the few TeV mass region, as in $gg \to \tilde{g}\tilde{g}$ [123]. It is also important for testing QCD, as factorisation and scales, as well as electroweak effects at large x in a future critical comparison of such ep with LHC pp data as for jets, see also [121]. Similarly, surprises may result from inclusive with jet LHeC data comparisons, not considered here. PDF physics rests on controlling and testing the underlying theory.

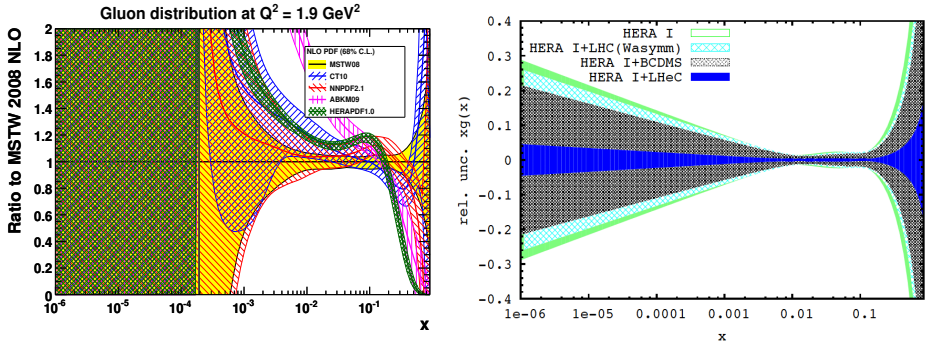

Figure 1-4. *Uncertainty of the gluon distribution at $Q^2 = 1.9\,GeV^2$ as a function of Bjorken x, see text. The LHeC PDF set, corresponding to the inner blue error band, is available on LHAPDF.*

1.2.5.2 Final Remark

It is important to emphasize that while the PDF analysis presented here serves as a valid starting point for comparison with existing PDFs, the LHeC has a unique potential to release the underlying simplifying assumptions and to provide a radically different and novel way to determine the PDFs: with the consideration

of the direct measurements of the strange, charm and beauty PDFs, perhaps even the top PDF, and with the addition of tagged eD data, it will be possible to analyze the behavior of not just 4 suitable combinations of PDFs but to determine the full set for the first time with crucial direct input, for example for the valence quarks at high x from high statistics CC data, at low x from electroweak structure functions or the light quarks independently of each other using ep and en and CC data. Therefore with the LHeC the world of PDFs will be radically changed. The present study of uncertainty to this extent is an illustration only and initially rather narrow in scope. It yet becomes evident that with the LHeC the development of QCD will hugely progress and the LH(e)C can be turned into a precision Higgs facility. Not excluded that electromagnetic substructure appears of the heaviest now elementary particles. Finally, the anticipated investment into highest LHC luminosity will be underpinned by the necessary precision QCD and PDF measurements by the LHeC without which highest mass limits must remain weaker and interpretations of subtle new features possibly uncertain. The LHeC appears as an impressively luminous, very important upgrade to the LHC with which the symmetry between pp, ep and may be e^+e^- can be restored at TeV energies, which appeared to be so fruitful, when the TeVatron, HERA and LEP/SLC eventually established the Standard Model of particle physics.

1.3 The strong coupling

Strong coupling constant α_s is one of the fundamental parameters of QCD. The coupling constant itself is not a physical observable, but a quantity defined in the context of perturbation theory, which enters predictions for experimentally-measurable observables. The size of α_s is not given by theory, but must be determined by experiments. The α_s value can be extracted from experimental measurements at e^+e^-, ep, pp, and $p\bar{p}$ colliders, as well as from Lattice QCD calculations. A recent review on the measurements of the strong coupling constant may be found in the 2012 PDG review [63]. The current world average presented in the 2012 PDG review is:

$$\alpha_s(M_Z) = 0.1184 \pm 0.0007$$

which has 0.6% relative uncertainty and is summarized in Fig. 1-5. As demonstrated in [63], the central value of the world average of $\alpha_s(M_Z)$ is rather stable against different inputs to this average. The result from lattice calculations, which has the smallest assigned uncertainty, agrees well with the exclusive average of the other results; however, it largely determines the size of the overall uncertainty. In spite of this relatively precise result, the uncertainty on α_s still contributes significantly to many QCD predictions. The precise determination of α_s would play an important role for many future energy frontier studies.

Below we discuss future possibilities to further improve the determination of α_s with measurements at the LHC and future accelerator facilities and with lattice QCD calculations. Given the current $\alpha_s(M_Z)$ uncertainty, the main theme is set to see if and/or how we can potentially reduce its uncertainty to the level of 0.1% relative or 0.0001 absolute uncertainties [64].

1.3.1 Strong coupling constant from e^+e^- data

Various studies on α_s have been performed using e^+e^- annihilation data. They include the determination of α_s from hadronic τ decays, heavy quarkonia decays, event shapes, jet rates, and hadronic Z decay rate. Future prospects with some of these approaches are discussed below.

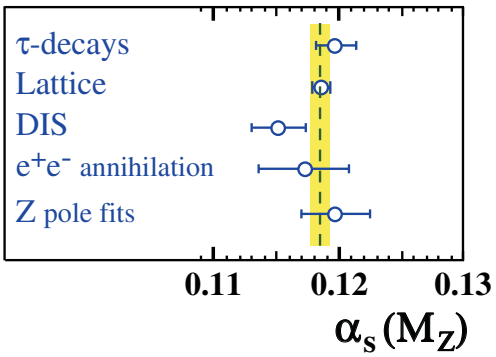

Figure 1-5. *Summary of values of $\alpha_s(M_Z)$ obtained for various sub-classes of measurements. The world average value of $\alpha_s(M_Z) = 0.1184 \pm 0.0007$ is indicated by the dashed line and the shaded band. Figure taken from [63].*

1.3.1.1 Hadronic final states of e^+e^- annihilations

Jet rates and event shapes have a high sensitivity to α_s, and they have been studied extensively in the past. For these observables, the theoretical predictions are calculated up to NNLO and the resummation is achieved up to NNLL or N^{3}LL.

The typical experimental uncertainty for these measurements is about 1%, and it is considered that improvements should be possible. The haronization uncertainty estimated based on the difference between various hadornization models is typically 0.7–1.5%. And, the theoretical uncertainties for the scale choice and variation, matching with resummed calculations, and quark mass effects are typically 3–5%. By the time when the next generations of e^+e^- colliders come online, we expect that both theoretical and hadronization uncertainties will reduce; however, going well below 1% would be quite challenging.

1.3.1.2 Hadronic W/Z decay widths from e^+e^- annihilations

An accurate determination of α_s may be obtained from the precise experimental measurement of hadronic Z decays. An advantage of using such inclusive observables is that the theoretical predictions are known to NNNLO **??** and non-perturvative effects are strongly suppressed. The ratio R_Z of the partial width of the Z into hadrons to that to one massless charged lepton flavour may be expressed by:

$$R_Z(R_l^0) \equiv \frac{\Gamma(Z \to \text{hadrons})}{\Gamma(Z \to \text{leptons})} = R_Z^{\text{EW}} N_C (1 + \delta_{\text{QCD}} + \delta_{\text{m}} + \delta_{\text{np}}), \tag{1.3}$$

$$\delta_{\text{QCD}} = \sum_{n=1}^{4} c_n \left(\frac{\alpha_s}{\pi}\right)^n + \mathcal{O}(\alpha_s^5), \quad c_1 = 1,\ c_2 = 0.76264,\ c_3 = -15.490, c_4 = -68.241,$$

$$\delta_{\text{m}} \sim \mathcal{O}\left(\frac{m_q^2}{M_Z^2}\right), \qquad \delta_{\text{np}} \sim \mathcal{O}\left(\frac{\Lambda^2}{M_Z^4}\right).$$

where the δ_{QCD}, δ_{m}, and δ_{np} terms are for the QCD, mass, and non-purtrubative corrections, respectively.

The latest result from the LEP electroweak working group on R_Z is $R_l^0 = 20.767 \pm 0.025$ [65], whose relative uncertainty is 0.12%. This translates to the value of $\alpha_{\rm s}(M_{\rm Z})$ as [64]:

$$\begin{aligned}\alpha_{\rm s}(M_{\rm Z}) &= 0.1226 \pm 0.0038(\exp)\,{}^{+\,0.0028}_{-\,0.0005}(\mu = {}^{2}_{0.25}M_Z)\,{}^{+\,0.0033}_{-\,0.0}(M_H = {}^{900}_{100}\ \text{GeV}) \\ &\quad \pm 0.0002(M_{\rm top} = \pm 5\ \text{GeV}) \pm 0.0002(\text{renormal. schemes}) \\ &= 0.1226\,{}^{+\,0.0058}_{-\,0.0038}.\end{aligned}$$

The relative uncertainty on R_l^0 increases by a factor of 25 for the relative uncertainty on $\alpha_{\rm s}(M_{\rm Z})$, because $c_1 \frac{\alpha_{\rm s}(M_{\rm Z})}{\pi} \sim 0.04 = \mathcal{O}(1/25)$ in Eq. (1.3). Since the uncertainty due to the Higgs mass dependence is no longer relevant, the top quark mass dependence is negligible, and the pQCD scale uncertainty from latest NNNLO calculations [67, 68] is only 0.0002 on $\alpha_{\rm s}(M_{\rm Z})$, the question comes down to if a future Z factory can measure Γ_Z at a precision of ~ 0.1 MeV or R_l^0 with an absolute precision of ~ 0.001. This feasibility depends on the precision on Z line shape observables, which may be achieved by future Z factories.

The LEP measurement of $R_l^0 = 20.767 \pm 0.025$ [65] is mainly limited by lepton statistics. With $\sim 10^{12}$ Z statistics expected from TLEP [69] and assuming the selection efficiency uncertainties scale with statistics, one might expect reduction of the uncertainty by a factor of ~ 200. At this level of precision, we will have to consider many subtle systematic uncertainties and a detailed analysis would be necessaary. The R_l^0 measurement is sensitive to the electroweak vertex correction δ_b; however, it can be constrained by the direction extraction of $R_b = \Gamma(Z \to b\bar{b})/\Gamma(Z \to \text{hadrons})$, so this is not expected to be a limitation. In order to achieve the absolute 0.0001 uncertainty on $\alpha_{\rm s}(M_{\rm Z})$, about a factor of 30 reduction in the uncertainty is necessary. This will require a lot of work and challenging, but the TLEP target goal of the measurement of R_l^0 with the relative precision of $< 10^{-5}$ meets this requirement. This would be an interesting possibility to explore [69].

Another interesting possibility suggested is to use the W hadronic width, i.e. $B_h \equiv (\Gamma_{\rm had}/\Gamma_{\rm tot})_W$, which we can extract by measuring the branching fraction of WW events to the $l\nu\, l\nu$, $l\nu\, qq$, and $qq\, qq$ final states. The previous LEP measurement of $B_h = 67.41 \pm 0.27$ [66] was limited by WW event statistics of about 4×10^4 events. With 0.5×10^8 W pairs expected at TLEP and assuming that selection efficiency uncertainties scale with statistics, there may be a possibility to reduce the uncertainty on B_h by factor ~ 70 and the absolute uncertainty on $\alpha_{\rm s}(M_{\rm Z})$ down to ~ 0.0002. It is an interesting possibility of the proposed TLEP facility.

1.3.2 Strong coupling constant at hadron colliders

The strong coupling constant has been extracted from measurements at hadron colliders as well. The results on the strong coupling constant from hadron collider jet data are based on the $p_{\rm T}$-dependence of the inclusive jet cross section measurements by the CDF [70], D0 [71], and ATLAS [73] Collaborations, the jet angular correlations by the D0 Collaboration [72], and the ratio of the inclusive 3-jet and 2-jet cross sections by the CMS Collaboration [74]. One of the complexities of the hadron-hadron environment is that it is hard to disentangle the extraction of the value of the strong coupling constant from the uncertainties in the gluon distribution, that can be signficant in the relevant x-range. The most precise measurement to date, $\alpha_{\rm s}(M_{\rm Z}) = 0.1161\,{}^{+\,0.0041}_{-\,0.0048}$, is from the inclusive jet cross section measurement from D0, and the uncertainty is dominated by the experimental uncertainties from the jet energy calibration, the $p_{\rm T}$ resolution, and the integrated luminosity, and as well as the uncertainties on non-purturbative corrections and the renormalization and factorization scales.

The recent result on $\alpha_{\rm s}(M_{\rm Z})$ from CMS based on $t\bar{t}$ cross section [75] yielded $\alpha_{\rm s}(M_{\rm Z}) = 0.1178\,{}^{+\,0.0033}_{-\,0.0032}$ based on full NNLO QCD calculation on the $t\bar{t}$ cross section. This is the first determination of the strong coupling constant from top-quark production and shows the best precision among hadron collider measurements.

There have been signifiant developments in measurements at the hadron colliders, and we expect that future LHC measurements will improve the precision on $\alpha_{\rm s}(M_{\rm Z})$ further; however, given the fact that the precision is limited by the experimental systematic uncertainty and the scale uncertainty; it will be challenging to achieve $< 1\%$ relative uncertainty on $\alpha_{\rm s}(M_{\rm Z})$. Nevertheless, the improved precision from hadron collider data at relatively high-Q is important for the robustness of $\alpha_{\rm s}$ determination and testing the running of $\alpha_{\rm s}$ and asymptotic freedom, as the current world average of $\alpha_{\rm s}(M_{\rm Z})$ is driven by low-Q measurements.

1.3.3 Strong coupling constant at LHeC

Two independent fit approaches have been undertaken in order to verify the potential of the LHeC to determine α_s. These analyses used a complete simulation of the experimental systematic errors of the NC and CC pseudo-data and higher order QCD fit analysis techniques, see the CDR [120] for details. The total experimental uncertainty on α_s is estimated to be 0.2 % from the LHeC alone and 0.1 % when combined with HERA. Relying solely on inclusive DIS ep data at high Q^2, this determination is free of higher twist, hadronic and nuclear corrections, unlike any of the recent global QCD fit analyses. There are known further, parametric, uncertainties in DIS determinations of α_s. These will be much reduced with the LHeC as it resolves the full set of parton distributions, $u_v,\ d_v,\ \overline{u},\ \overline{d},\ s,\ \overline{s},\ c,\ b$ and xg for the first time, providing x and Q^2 dependent constraints not "just" through the fit procedure.

1.3.4 Strong coupling constant from lattice QCD

1.4 Higher-order corrections

The current standard for most theoretical predictions at hadron colliders is NLO, with a small number of calculations extended beyond this to NNLO. In this section we review the behavior of some these predictions for LHC operations at 14 TeV and for proton-proton collisions at 33 and 100 TeV. We also summarize recent results on extending the predictions for one of the most important cross sections, Higgs boson production by gluon fusion, to N^{3}LO. We also provide an overview of the highest-priority perturbative calculations, ones that could feasibily be tackled in the next 5–10 years.

1.4.1 NLO cross sections at 14, 33 and 100 TeV

As a first step towards investigating the physics potential of future proton-proton colliders, it is interesting to investigate the center-of-mass energy dependence of notable cross-sections at such machines. Figure 1-6 shows the predicted cross sections for a selection of basic processes, ranging over twelve orders of magnitude from the total inelastic proton-proton cross section to Higgs boson pair-production. For inclusive jet and direct photon production, 50 GeV transverse momentum cuts are applied to the jet and the photon respectively. The cross sections presented in this figure have been calculated at next-to-leading order in QCD using the MCFM program [31], or taken from the European Strategy report [60] (in the case of Higgs cross sections).

The growth of the cross-sections with $\sqrt{s}$ largely reflects the behavior of the underlying partonic luminosities. For instance, the top pair cross section is dominated by the partonic process $gg \to t\bar{t}$ and the gluon-gluon

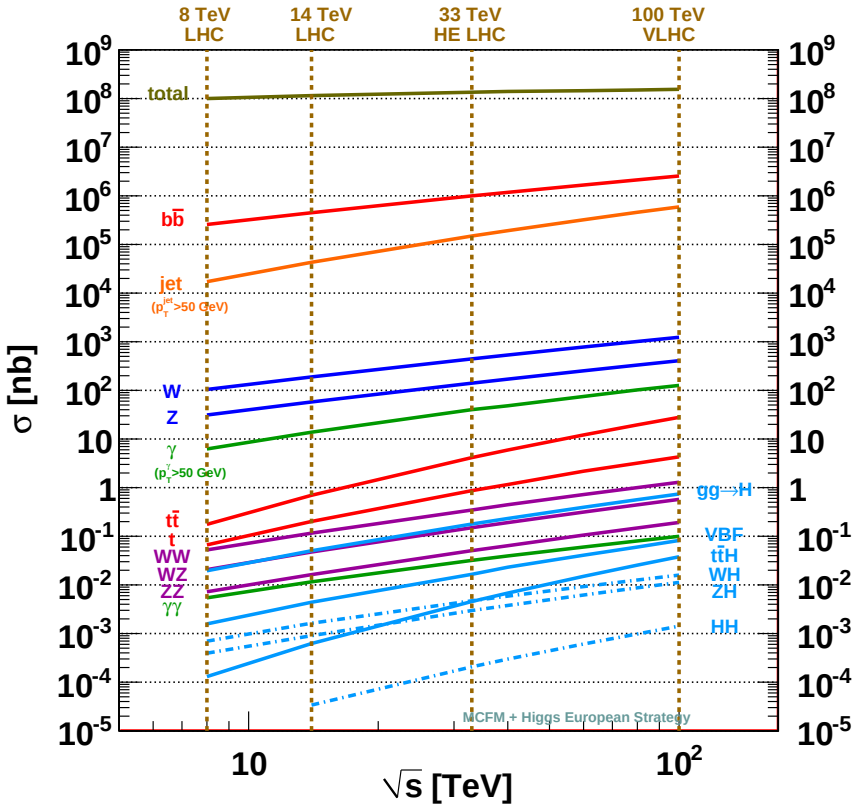

Figure 1-6. *Cross section predictions at proton-proton colliders as a function of center-of-mass operating energy, $\sqrt{s}$.*

luminosity rises significantly at higher values of $\sqrt{s}$. The same holds true for the Higgs production channel $t\bar{t}H$ but, in contrast, the associated production channels are dominated by quark-antiquark contributions and rise much more slowly. The different behavior means that, unlike at current LHC operating energies, the $t\bar{t}H$ channel becomes the third-largest Higgs production cross section at 33 TeV and above. As a figure of merit for estimating the difficulty of observing the Higgs pair production process it is not unreasonable to consider the ratio of its cross section to the top pair cross section. For instance, for many of the possible Higgs boson decays the final states could receive significant background contributions from the top pair process. The fact that both processes are predominantly gluon-gluon induced means that this measure is approximately constant across the range of energies considered. It is therefore not clear that the prospects for extracting essential information from the Higgs-pair process would be significantly easier at a higher-energy hadron-collider.

A different sort of contribution to event rates can also be estimated from this figure. The contribution of double parton scattering (DPS) – where a single proton-proton collision is responsible for two hard events – can be estimated by,

$$\sigma_{XY}^{\mathrm{DPS}} \approx \frac{\sigma_X \sigma_Y}{15\ \mathrm{mb}}\ . \tag{1.4}$$

In this equation the DPS contribution for the final state XY is related to the usual cross sections for individually producing final states X and Y using the effective DPS cross section. This cross section appears to be approximately independent of energy up to 8 TeV and is approximately 15 mb (for example, see Ref. [32] for a recent measurement at 7 TeV). Of course the uncertainty on the effective cross section, and indeed on the accuracy of equation (1.4) itself, is such that this should be considered an order-of-magnitude estimate only. A particularly simple application of this is estimating the fraction of events for a given final state in which there is an additional DPS contribution containing a pair of b-quarks. This fraction is clearly given by the ratio, $\sigma_{b\bar{b}}/(15\text{ mb})$. From the figure this fraction ranges from a manageably-small 2% effect at 8 TeV to a much more significant 20% at 100 TeV. More study would clearly be required in order to obtain a true estimate of the impact of such events on the physics that could be studied at higher energies, but these simplified arguments can at least give some idea of the potentially troublesome issues.

As an example of the behavior of less-inclusive cross sections at higher energies, Figure 1-7 shows predictions for $H + n$ jets $+ X$ cross sections at various values of $\sqrt{s}$ and as a function of the minimum jet transverse momentum. The cross sections are all normalized to the inclusive Higgs production cross section, so that the plots indicate the fraction of Higgs events that contain at least the given number of jets. The inclusive Higgs cross section includes NNLO QCD corrections, while the 1- and 2-jet rates are computed at NLO in QCD.

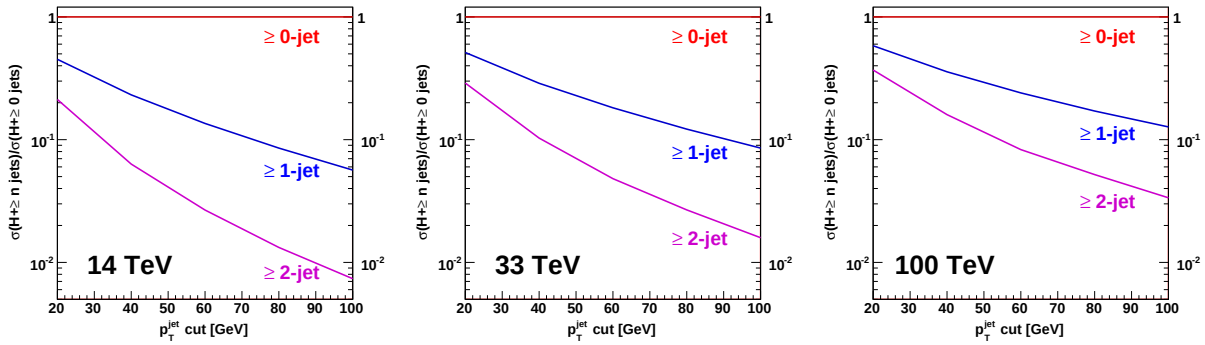

Figure 1-7. *Cross sections for the production of a Higgs boson produced in association with n or more jets, for $n = 0, 1, 2$, normalized to the inclusive Higgs cross section ($n = 0$). Cross sections are shown as a function of the minimum jet p_T and are displayed for a proton-proton collider operating at 14 TeV (left), 33 TeV (center) and 100 TeV (right).*

The extent to which additional jets are expected in Higgs events is clearly strongly dependent on how the jet cuts must scale with the machine operating energy. For instance, consider a jet cut of 40 GeV at 14 TeV, a value in line with current analysis projections. For this cut, approximately 20% of all Higgs boson events produced through gluon fusion should contain at least one jet and the fraction with two or more jets is expected to be around 5%. To retain approximately the same jet compositions at 33 and 100 TeV requires only a modest increase in the jet cut to 60 and 80 GeV respectively.

At higher operating energies it is especially interesting to compare predictions produced using the standard perturbative expansion, here at NLO, with alternative formalisms that directly appeal to the high energy limit. One such formalism is encoded in the program HEJ ("High Energy Jets") [57, 58] that implements a resummation scheme based on the factorisation of scattering amplitudes in the high energy limit. For this study we investigate predictions for $H + 2$ jet events, with particular interest in the region where two of the jets are separated by a large rapidity span. As well as being relevant for separating the gluon fusion and

vector boson fusion processes, this region is expected to be particularly sensitive to differences between the predictions of NLO QCD and HEJ [61]. Jets are reconstructed using the k_T algorithm with $D = 0.6$ and $|y| < 5$. In the first scenario we consider a minimum transverse momentum cut of 40 GeV for operating energies of 14, 33 and 100 TeV. In the second scenario the jet cut is doubled to 80 GeV at 33 TeV and again to 160 GeV at 100 TeV.

The results of this study are shown in Figure 1-8. Predictions are shown for the ratio of inclusive 3-jet to inclusive 2-jet events, as a function of the rapidity difference between the two most widely-separated jets. The uncertainty band is obtained by varying the scale choice by a factor of two about the central value ($H_T/2$, where H_T is the sum of the total transverse momentum of all objects in the final state).

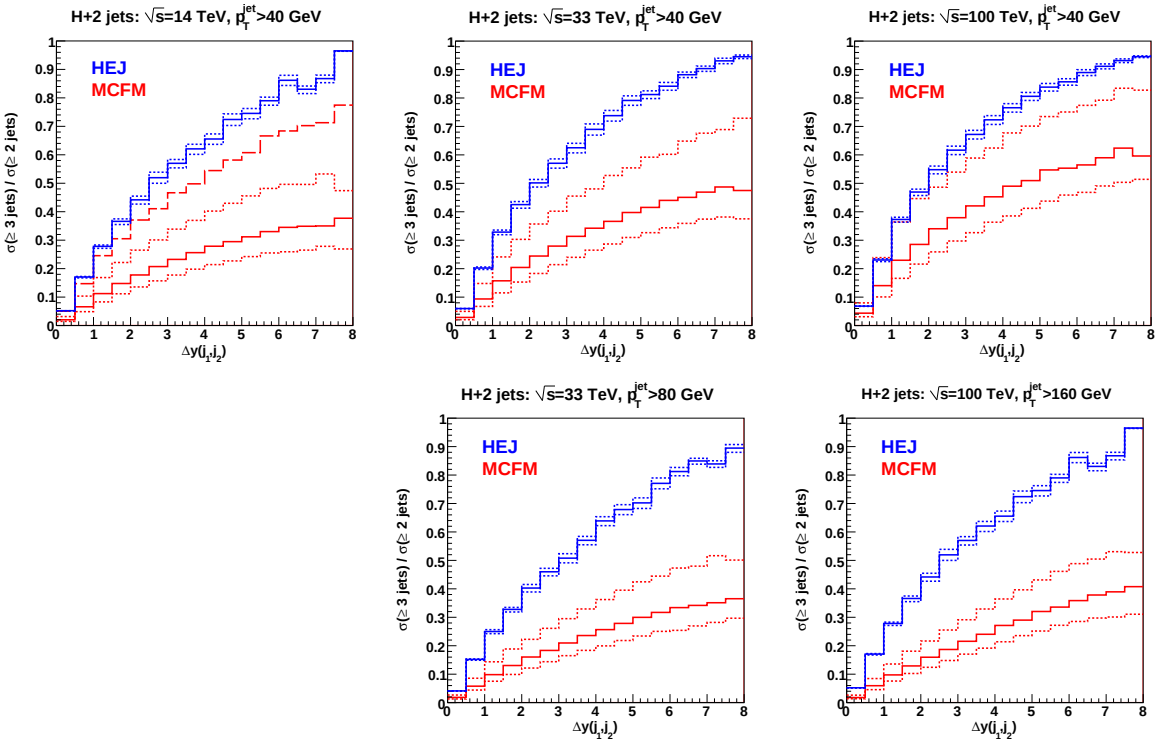

Figure 1-8. *The ratio of number of events that contain at least three jets to the number that contain two jets, as a function of the rapidity difference between the two most widely-separated jets. Predictions are obtained using the NLO calculation of the $H + 2$ jet process and are shown at three operating energies. The jet transverse momentum cut is at 40 GeV (top), or scales with the operating energy (bottom).*

In all five scenarios, the predictions from HEJ for the ratio of 3-jet to 2-jet events rises faster and reaches a higher value than the prediction from the NLO calculation as the rapidity span of the event increases. This is the region where the higher-order corrections included in HEJ become significant.

As the collider energy is increased while the jet p_T cut is kept constant the phase space for the production of higher numbers of jets increases. This is illustrated in the top row of Figure 1-8, where it can be seen that the value of the ratio increases in both descriptions. Where the jet p_T cut is also increased, the ratio remains more stable.

The HEJ predictions include higher-order logarithmic corrections which stabilise the result with respect to scale variations. The NLO MCFM results are much more sensitive to changes in the scale as can be seen from the wider uncertainty bands. This is further illustrated in the first plot (for collider energy 14 TeV and jet $p_T > 40$ GeV) where the additional dashed line shows the MCFM result for an even lower scale choice of $H_T/6$. A typical H_T value for these events is around 250 GeV, so this choice is closer to the scale of the jet p_T. The predictions for this choice are closer to the HEJ predictions especially at small values of Δy.

1.4.2 Extrapolation from existing NLO results

The progress within the last 5 years in the calculation of NLO corrections for complex final states has been truly impressive, as witnessed for example by the calculation of $W + 5$ jets by the Blackhat+Sherpa collaboration [62]. Of course, there is a limit, as increasing the number of partons in the final state by definition increases the complexity of the calculation, while the physics reward (typically) decreases. Within a matrix-element + parton shower framework, additional jets can be added either at leading order or through the parton shower. In addition, there are heuristic tools that can be developed to extrapolate cross sections for higher jet multiplicity based on the patterns observed at lower jet multiplicity. For instance, known results for $W + 2$ through $W + 5$ jet production can be used to assess the scaling behavior of the $W + n$ jet cross sections [6] Defining the quantity $R^{\pm} = \sigma(W^{\pm} + n \text{ jets})/\sigma(W^{\pm} + n - 1 \text{ jets})$, Blackhat+Sherpa have developed predictions for this ratio for $n \geq 3$, in pp collisions at 7 TeV, for jets with $p_T > 25$ GeV. The predictions are:

$$R^{+}_{\text{NLO}} = 0.0263 \pm 0.009 - (0.009 \pm 0.003)\, n$$
$$R^{-}_{\text{NLO}} = 0.0248 \pm 0.008 - (0.009 \pm 0.002)\, n$$

From these formulae, the cross sections at NLO for $W + 6$ or 7 jets can be predicted, without any actual calculation. Of course, such scaling formulae are strongly dependent on the kinematic regions being considered, but can easily be re-assessed for different cuts or center-of-mass energies.

1.4.3 Computational complexity

The advances of NLO and NNLO multi-leg calculations have resulted in programs that are (1) very complex and (2) very time-consuming to run using the resources available to a typical user. It can thus be difficult for a full dissemination of the theoretical results to the experimental community. The Blackhat+Sherpa collaboration has partially addressed these issues by releasing results for $W/Z + n$ jets in ROOT ntuple format, with all information needed for calculation of physical cross sections with a variety of jet parameters and cuts. In addition, the results can be re-weighted for different scales and different PDFs. The cost is the presence of very large outputs, but subdivided into files of a few GB that are ideal for parallel processing. Ntuples are probably not practical, though, for some of the more complex NNLO calculations, such as inclusive jet production, where the number of files needed would be prohibitive. Making the resultant program user-friendly, though, can take a great deal of time.

An alternative is to make such complex programs available to the user on high performance computing platforms, which inherently have much greater processing and storage capabilities; in addition, the programs may be pre-compiled by the authors insuring that the calculation is run correctly. Initial tests of HPC

[6] $W + 1$ jet behaves differently because of missing production channels and kinematic differences.

platforms have been successfully carried out during the Snowmass workshop. We have shown weak scaling up to 16000 cores on IBM BlueGene/Q, up to 8192 cores on CRAY XK7, and strong scaling up to 1024 cores on CRAY XK7 using Sherpa. Another possibility for large-scale production runs may be the Open Science Grid. The first attempt to introduce it to the pQCD community may have failed, but it has great potential to harvest existing resources.

1.4.4 Improvements to matrix element and parton shower matching

General-purpose event generators have been undergoing tremendous development over the past years. Both the fixed-order and logarithmic accuracy underpinning their simulations of perturbative QCD have been improved in order to match increased precision needs in the experiments.

The basis for the these developments was established by the MC@NLO technique [39], which matches NLO QCD calculations to parton showers, such that fully differential events can be generated at the particle level. The POWHEG [40, 41] method was later introduced to eliminate negative weights from simulations.

Parton-shower matched predictions have been provided for some of the most challenging NLO calculations to date, including, for example, $pp \to W + 3$ jets [49] and $pp \to t\bar{t}$+jet [50]. The current limitation in matching to even higher multiplicity processes is not of algorithmic nature, but purely computational, and it is related to the memory consumption of executables. Fixed-order calculations benefit from the fact that they can be split into different parts, corresponding to Born, virtual correction, integrated infrared subtractions and real-emission correction minus real subtraction. Due to the intricate interplay between real and virtual corrections in MC@NLO and POWHEG, such a splitting is harder to achieve when matching to a parton shower.

Different proposals were made to combine MC@NLO simulations of varying jet multiplicity into inclusive event samples [42, 43]. They are natural extensions of the CKKW(-L) [44, 45] and MLM [46] leading-order merging schemes to the next-to-leading order, respectively. Another, entirely independent method was introduced earlier, which relies on a different subtraction scheme [47, 48]. The simulations provided by these new techniques can be used to obtain NLO-accurate predictions for different jet multiplicities at the same time.

Achieving this level of fixed-order accuracy has been a priority in the development of Monte-Carlo event generators for more than a decade. The current technology has undoubtedly benefited greatly from the advances in computing fixed-order NLO QCD corrections at large jet multiplicity in a fully automated manner. These calculations provide the parton-level input for the new merging methods.

NLO-merged predictions have been provided for $pp \to W/Z$+jets with up to two jets described at NLO accuracy [42], $pp \to H$+jets in gluon fusion, with up to one jet at NLO accuracy [48, 43] and $pp \to t\bar{t}$+jets with up to one jet at NLO accuracy [43, 51]. All related implementations are fully automated and can, in principle, be used for any type of reaction. However, because MC@NLO parton-level predictions are needed as an input, the current limitations are identical to those for MC@NLO. They are not due to algorithmic deficiencies, but mostly due to memory constraints on production systems and restrict the usage of the methods to processes with fewer than four light jets in the final state computed at NLO.

It is conceivable that working techniques for matching NNLO fixed-order calculations to parton-shower simulations will be constructed in the near to mid-term future. Such a matching, which could be dubbed 'MC@NNLO', would further stabilize predictions for the differential cross section at lowest multiplicity, and eliminate the unitarity violation observed in most NLO merging methods in a natural way.

An alternative technique already exists, which does not rely on a modified subtraction scheme to construct counterterms for fixed-order calculations, but on constructing counterterms for the parton shower, at the order at which the shower is to be matched [47]. This is very easy to achieve. The method has been used as proof of principle to provide NNLO matched predictions for $e^+e^- \to$jets production [47].

At the same time that matching to fixed-order NNLO calculations is being developed, the logarithmic accuracy of parton shower simulations must be improved systematically, in order not to degrade the precision of the fixed-order result after matching. This involves two developments:

Firstly, corrections which are sub-leading in the number of colors, N_c, must be included. A proposal to do this was formulated some time ago [52], but first steps to implementation were taken only recently [53, 54]. The importance of sub-leading N_c corrections in processes with non-trivial color structure at Born level was observed in an analysis of the $t\bar{t}$ forward-backward asymmetry [51]. Respecting the full color structure during parton evolution will allow to include all next-to-leading logarithmic effects in the parton shower, in a manner that is independent of the actual evolution variable, and therefore does not rely on angular ordering.

Secondly, it will be beneficial to systematically extend parton-showers to higher logarithmic accuracy, for example by including higher-point splitting functions. An alternative approach, based on the matching of parton showers to analytic calculations at higher logarithmic accuracy also seems promising. Such an approach was used already to generate predictions for the thrust distribution and several event shapes in $e^+e^- \to$jets [55]. First results for $pp \to e^+e^-$ have been reported [56].

Logarithmic enhancements of the cross section at high energy, which are resummed in the HEJ framework [57, 58] could be crucial to understanding the structure of multi-jet events at the LHC. Including these contributions in event generators may become important [59].

1.4.5 Beyond NNLO: Higgs boson production

Small x "BFKL" (or high-energy) resummation and large x "Sudakov" (or threshold, or soft-gluon) resummation provide information on the all-order behaviour of a wide class of hadron collider observables in two opposite kinematic limits. Because the Mellin transform of a partonic cross section $\sigma(N, \alpha_s(M^2))$ is an analytic function of the variable N which is conjugate to the longitudinal momentum scaling variable (usually called x or τ), this information provides powerful constraints on the unknown higher order perturbative corrections to the cross-section.

The use of resummation to determine approximate higher order perturbative corrections has a long history, and, in particular, approximate NNLO jet cross sections determined using results from threshold resummation [38] are routinely used in PDF fits. Recently, in Ref. [33] it was suggested that especially accurate results can be obtained if maximal use is made of analyticity constraints, by not only combining information from differenmt kinds of resummation, but also making sure that the known all-order analytic properties of the cross section are reproduced as much as possible. So, for instance, while as $N \to \infty$ $\sigma(N, \alpha_s(M^2)) \sim \sum_k (\alpha_s(Q^2) \ln^2 N)^k$, the cross section is expected to have poles, and not cuts when $N = 0$, and indeed, a more detailed analysis reveals that the logarithmic behaviour of the cross section only arises through functions such as $\psi_0(N)$, which indeed has a simple pole at $N = 0$ even though $\psi_0(N) \sim \ln N$ as $N \to \infty$.

In Ref. [33] it was shown that indeed this approach leads to a very good approximation to the known NLO and NNLO expressions for the total cross section for Higgs production in gluon fusion with finite m_t (in

particular, rather better than it would be found by simply expanding out the standard resummed result of Ref. [34]). An approximate expression for the N3LO correction to the cross section was then constructed.

The full N^{3}LO Higgs production cross section at the LHC at $\sqrt{s} = 8$ TeV, with $m_H = 125$ GeV was found to be (using the NNPDF2.1 PDF set with $\alpha_s(M_z) = 0.119$)

$$\begin{aligned}\sigma^{\mathrm{N^3LO}}_{\mathrm{approx}}(\tau, m_H^2) &= \sigma^{(0)}(\tau, m_H^2)\left[\sum_{ij}\left(\delta_{ig}\delta_{jg} + \alpha_s K^{(1)}_{ij} + \alpha_s^2 K^{(2)}_{ij}\right) + \alpha_s^3 K^{(3)}_{gg,\mathrm{approx}}\right] \\ &= \left(22.61 \pm 0.27 + 0.91 \cdot 10^{-2}\bar{g}_{0,3}\right)\ \mathrm{pb} \qquad \text{for } \mu_R = m_H \\ &= \left(24.03 \pm 0.45 + 1.55 \cdot 10^{-2}\bar{g}_{0,3}\right)\ \mathrm{pb} \qquad \text{for } \mu_R = m_H/2,\end{aligned} \tag{1.5}$$

where the error shown is an estimate of the uncertainty in the approximation procedure, and the coefficient $\bar{g}_{0,3}$ is unknown. The known perturbative behaviour of the coefficients $g_{0,i}$, which provide constant corrections to the cross section (i.e. neither logarithmically enhanced nor power-suppressed as $N \to \infty$) suggests that $\bar{g}_{0,3}$ is possibly of order ten. The renormalization scale dependence of the contribution from the gluon-gluon channel to the cross section is shown in Figure 1-9 for various choices of the collider energy (red band), and compared to the exact LO, NLO, and NNLO results, and also to the a different soft approximation and its collinear improvement (see below). Note that the factorization scale dependence of the result is known to be essentially negligible even at LO, more so at NLO and NNLO.

The main features of this approximate result are the following:

- The perturbative expansion converges quite slowly: in particular, it is clear that at each order the next-order result is not cointained within the range found varying the scale by a factor two about either m_H or $m_H/2$.
- The perturbative expansion converges better as the collider energy increases. The reason for this can be understood by computing the value of N which dominates the cross-section [35], which is fully determined by the collider energy and the Higgs mass, and then studying the perturbative behaviour of the cross section for the given value of N (see Figure 1-10).
- For all collider energies, the scale dependence is considerably reduced by the inclusion of the N^{3}LO corrections.
- The central prediction of Ref. [33], Eq. 1.5, amounts to a rather substantial correction, of order of 17% for $\mu_R = m_H$ at LHC 8 TeV.
- The N^{3}LO truncation of the resummed result of Ref. [34]) (also shown and labelled "N-soft" in Figure 1-9) together with its collinear improvement according to Ref. [36] (labelled "N-soft-coll") would predict a rather smaller correction to the NNLO result, of order of 6% for $\mu_R = m_H$.
- The whole NNLL correction to the NNLO result from Ref. [34] modifies the NNLO result by about 8%, 6% of which, as mentioned, comes from the N^{3}LO, and the remaining 2% or so from higher orders. This means that the resummation is perturbative in this region: it mostly amounts to a prediction for the N^{3}LO correction.
- The discrepancy between the prediction of a 6% correction N^{3}LO (expanding out the resummation of Ref. [34]) and a a 17% correction (using the approximation of Ref. [33]) is partly due to the choice of the value for the constant $\bar{g}_{0,3}$. In fact, using the value of the constant which is implicit in the resummed result of Ref. [34] reduces the N^{3}LO correction Eq. 1.5 from about 17% to about 12%. The remaning difference, which is thus by about a factor two for this scale choice, is due to the (allegedly more accurate) approximation of Ref. [33].

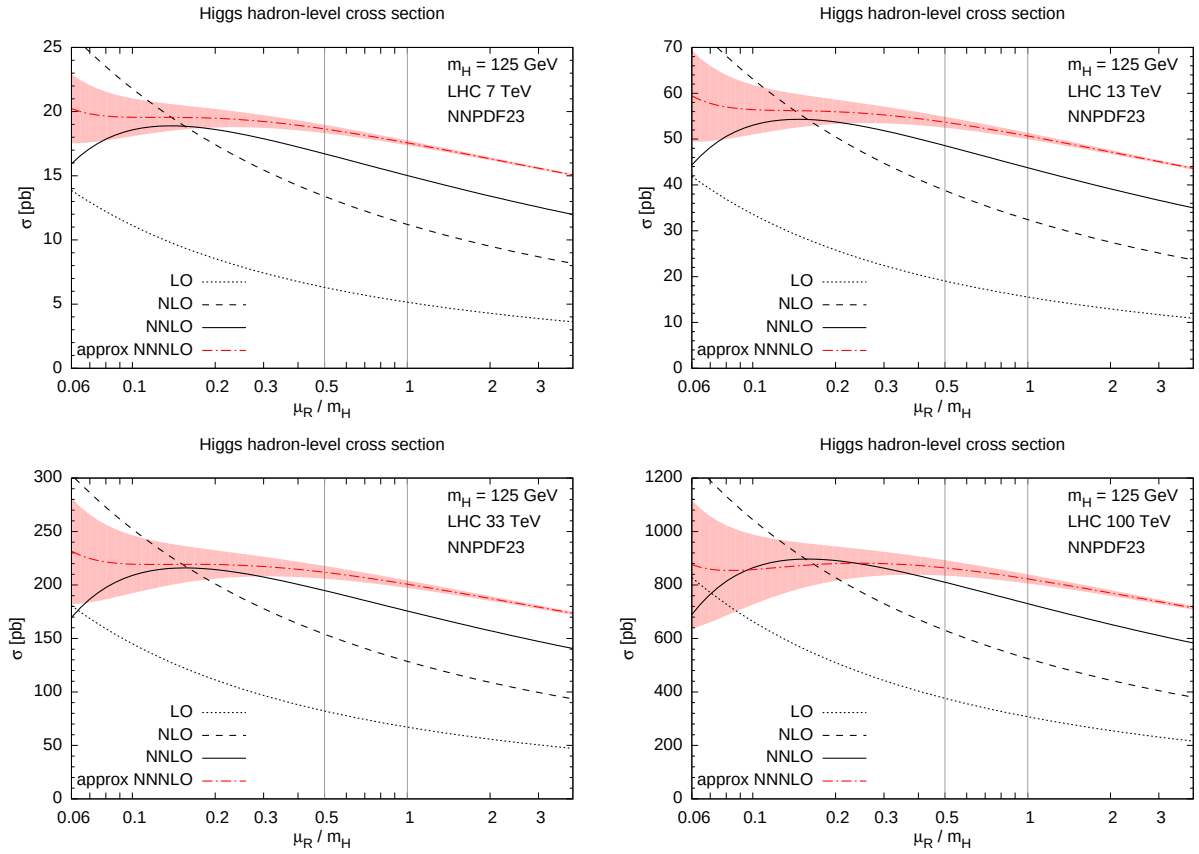

Figure 1-9. *Dependence on the renormalization scale of the LO, NLO, NNLO and approximate N^3LO contribution from the gluon-gluon channel to the total cross section for Higgs production at a proton-proton collider with four different values of the collider energy. The results shown are obtained using the NNPDF2.3 PDF set with $alpha_s(M_z) = 0.118$*

- The difference between the approximation of Ref. [33] and the expansion of the resummed result is mostly due to the fact that the soft approximation in Ref. [33] is designed to preserve the small N singularity structure. The explicit inclusion of the correct small N terms from the "BFKL" resummation has some effect in stabilizing somewhat the scale dependence at the very lowest edge $\mu_R/m_H < 0.1$ of the scale variation range of Figure 1-9, but it otherwise has a small impact.
- The scale dependence of the N^{3}LO result was also determined in Ref. [37] as a function of the value of the cross-section at the reference scale $\mu_R = m_H/2$. It was found that if this value is such that the scale dependence of the N^{3}LO is smaller than that of the NNLO, then the N^{3}LO is in the same ballpark as found in Ref. [33].

There are ongoing efforts to complete a full N^{3}LO calculation of the $gg \to H$ cross section, i.e. to provide the value of the coefficient $\bar{g}_{0,3}$ in equation 1.5. Given the slow convergence of the perturbative series for this process, a full calculation to this order may be necessary to achieve the needed theoretical precision for Higgs production, both for 14 TeV and for still higher energies.

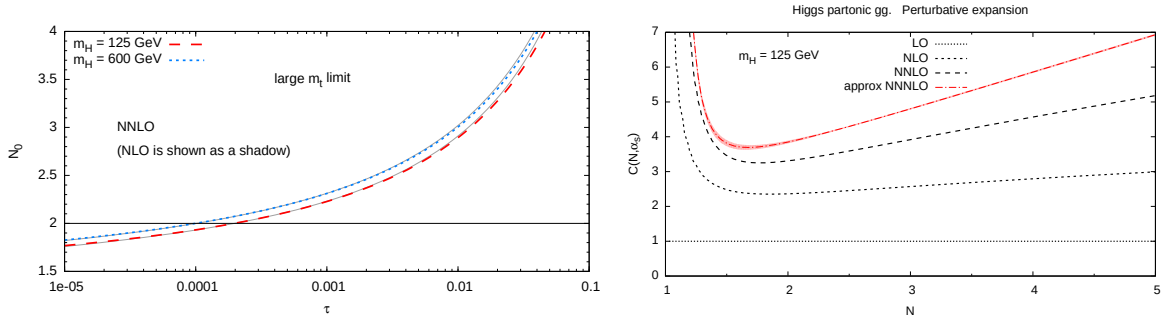

Figure 1-10. *Position of the saddle-point value of N which dominates the Mellin-space cross section for production of a 125 GeV Higgs boson in gluon fusion as a function of the collider energy (left), and perturbative expansion of the cross-section (right)*

1.4.6 Wishlist for higher order QCD and EW corrections

The Les Houches NLO wish list, consisting of calculations that were phenomenologically important for LHC physics, and were feasible but difficult to calculate at NLO in perturbative QCD, was started in 2005. After being incremented in 2007 and 2009 it was terminated in 2011. By 2011, every calculation on the wish list had been determined, and technology had advanced far enough that any reasonable multi-parton calculation could be carried out at NLO using semi-automated technology. In 2013, the NLO wish list was replaced by one at NNLO, the new calculational frontier; given the precision inherent at NNLO, many of the calculations on the list also involve the determination of electroweak corrections at NLO. The new wish list is shown in Tables 1-1, 1-2 and 1-3, giving the level to which the current calculation is known, and the level which is desired for full exploitation of physics at the LHC and higher energy hadron-hadron colliders. For the Higgs boson processes listed in Table 1-1 the improved calculations will enable more accurate extractions of Higgs couplings. The processes involving heavy quarks and jets, Table 1-2, will predominantly provide better extractions of pdfs. The vector boson processes given in Table 1-3 will be essential in investigating the precise nature of electroweak symmetry breaking – for instance by providing more accurate predictions for channels that are sensitive to vector boson scattering at high energy and to anomalous cubic and quartic gauge boson couplings.

Until recently, the start of the art for NNLO was the calculation of $2 \to 1$ processes. Within the last few years, several calculations of $2 \to 2$ processes have been completed. Indeed, the year 2013 has seen the completion of a number of landmark calculations at NNLO, namely the total cross section for top pair production [17] and first approximations of jet production [16] and the Higgs+jet process [30]. It is noteworthy that the wish list even contains $2 \to 3$ and $2 \to 4$ processes. Adding to the complexity is the need for the inclusion of decays for many of the massive final state particles. Given the recent progress in the field, it is difficult to speculate as to what length of time will be needed for the completion of this new list, but a period of 10 years may be a reasonable estimate.

Note that for many processes the higher order QCD and the higher order EWK corrections are currently known separately, while the desire is to have combined corrections, often at NNLO in QCD and NLO in EWK. One of the ambiguities in situations where the corrections are known separately is whether the two corrections are multiplicative or additive, i.e. whether the EWK corrections are affected by the (often) large QCD corrections. The degree to which the corrections are multiplicative or additive no doubt depends on the particular process and even on the observable within that process. The joint calculations posited here will resolve this ambiguity.

Process	known	desired	details
H	dσ @ NNLO QCD dσ @ NLO EW finite quark mass effects @ NLO	dσ @ NNNLO QCD + NLO EW MC@NNLO finite quark mass effects @ NNLO	H branching ratios and couplings
H + j	dσ @ NNLO QCD (g only) dσ @ NLO EW finite quark mass effects @ LO	dσ @ NNLO QCD + NLO EW finite quark mass effects @ NLO	H p_T
H + 2j	σ_{tot}(VBF) @ NNLO(DIS) QCD dσ(gg) @ NLO QCD dσ(VBF) @ NLO EW	dσ @ NNLO QCD + NLO EW	H couplings
H + V	dσ @ NNLO QCD dσ @ NLO EW	with $H \to b\bar{b}$ @ same accuracy	H couplings
t$\bar{t}$H	dσ(stable tops) @ NLO QCD	dσ(top decays) @ NLO QCD + NLO EW	top Yukawa coupling
HH	dσ @ LO QCD (full m_t dependence) dσ @ NLO QCD (infinite m_t limit)	dσ @ NLO QCD (full m_t dependence) dσ @ NNLO QCD (infinite m_t limit)	Higgs self coupling

Table 1-1. *Wishlist part 1 – Higgs (*V = W, Z*).*

Process	known	desired	details
t$\bar{t}$	σ_{tot} @ NNLO QCD dσ(top decays) @ NLO QCD dσ(stable tops) @ NLO EW	dσ(top decays) @ NNLO QCD + NLO EW	precision top/QCD, gluon PDF, effect of extra radiation at high rapidity, top asymmetries
t$\bar{t}$ + j	dσ(NWA top decays) @ NLO QCD	dσ(NWA top decays) @ NNLO QCD + NLO EW	precision top/QCD top asymmetries
single-top	dσ(NWA top decays) @ NLO QCD	dσ(NWA top decays) @ NNLO QCD (t channel)	precision top/QCD, V_{tb}
dijet	dσ @ NNLO QCD (g only) dσ @ NLO weak	dσ @ NNLO QCD + NLO EW	Obs.: incl. jets, dijet mass $\to$ PDF fits (gluon at high x) $\to \alpha_s$
3j	dσ @ NLO QCD	dσ @ NNLO QCD + NLO EW	Obs.: $R3/2$ or similar $\to \alpha_s$ at high scales dom. uncertainty: scales
γ + j	dσ @ NLO QCD dσ @ NLO EW	dσ @ NNLO QCD +NLO EW	gluon PDF γ + b for bottom PDF

Table 1-2. *Wishlist part 2 – jets and heavy quarks.*

Process	known	desired	details
V	dσ(lept. V decay) @ NNLO QCD dσ(lept. V decay) @ NLO EW	dσ(lept. V decay) @ NNNLO QCD + NLO EW MC@NNLO	precision EW, PDFs
V + j	dσ(lept. V decay) @ NLO QCD dσ(lept. V decay) @ NLO EW	dσ(lept. V decay) @ NNLO QCD + NLO EW	Z + j for gluon PDF W + c for strange PDF
V + jj	dσ(lept. V decay) @ NLO QCD	dσ(lept. V decay) @ NNLO QCD + NLO EW	study of systematics of H + jj final state
VV′	dσ(V decays) @ NLO QCD dσ(stable V) @ NLO EW	dσ(V decays) @ NNLO QCD + NLO EW	off-shell leptonic decays TGCs
gg $\to$ VV	dσ(V decays) @ LO QCD	dσ(V decays) @ NLO QCD	bkg. to $H \to VV$ TGCs
Vγ	dσ(V decay) @ NLO QCD dσ(PA, V decay) @ NLO EW	dσ(V decay) @ NNLO QCD + NLO EW	TGCs
Vb$\bar{\text{b}}$	dσ(lept. V decay) @ NLO QCD massive b	dσ(lept. V decay) @ NNLO QCD massless b	bkg. for VH $\to$ b$\bar{\text{b}}$
VV′γ	dσ(V decays) @ NLO QCD	dσ(V decays) @ NLO QCD + NLO EW	QGCs
VV′V″	dσ(V decays) @ NLO QCD	dσ(V decays) @ NLO QCD + NLO EW	QGCs, EWSB
VV′ + j	dσ(V decays) @ NLO QCD	dσ(V decays) @ NLO QCD + NLO EW	bkg. to H, BSM searches
VV′ + jj	dσ(V decays) @ NLO QCD	dσ(V decays) @ NLO QCD + NLO EW	QGCs, EWSB
$\gamma\gamma$	dσ @ NNLO QCD		bkg to $H \to \gamma\gamma$

Table 1-3. *Wishlist part 3 – EW gauge bosons* (V = W, Z).

1.4.7 Electroweak corrections and Sudakov logarithms

At the energies of future high-energy collider experiments the electroweak (EW) radiative corrections are generally expected to become more and more important since they are dominated by double and single logarithmic contributions (DL and SL, respectively) whose argument involves the ratio of the energy scale to the mass of the weak bosons. These corrections, termed Sudakov logs, are generated by diagrams in which virtual and real gauge bosons are radiated by external leg particles, and correspond to the soft and collinear singularities appearing in QED and QCD, i.e. when massless gauge bosons are involved. At variance with this latter case, the weak bosons masses act as a physical cutoff on these "singularities", so that virtual and real weak bosons corrections can be considered separately. Moreover, as the radiation of real weak bosons is in principle detectable, for those event selections where one does not include real weak bosons radiation the physical effect of virtual corrections is singled out, and can amount to several tens of per cent, or more. The one-loop Sudakov logs are naturally included in any complete calculation of NLO EW radiative corrections to a given process.

Often, these NLO electroweak high energy logs (Sudakov logs) can be a reasonable approximation for the full NLO electroweak corrections for a process. The leading term in the Sudakov form factor is given by $\alpha_{\rm w} \ln^2\left(Q^2/M_{\rm W}^2\right)$, where Q denotes the energy scale of the hard-scattering process, $M_{\rm W}$ is the W-boson mass, and $\alpha_{\rm w} = \alpha/\sin^2\theta_{\rm w} = e^2/(4\pi\sin^2\theta_{\rm w})$ with $\theta_{\rm w}$ denoting the weak mixing angle. This approach misses finite contributions of order α, but can work very well in the Sudakov regime, where s and $|t|$ are both large (¿¿m_W^2). In suitable kinematic regions, the electroweak Sudakov logs can lead to large negative corrections to cross sections. The net effect of electroweak corrections will depend on the relative size of electroweak tree-level contributions. This section covers specific calculations of electroweak corrections for pp→ dijet, inclusive W and Z, W/Z+jets, and WW production, at center-of-mass energies of 8, 14, 33 and 100 TeV, where the magnitude of the Sudakov leading log corrections is compared with the cross sections calculated at leading order in α_S. The section following discusses the implementation of Sudakov logarithmic effects by process-independent methods in the ALPGEN Monte Carlo.

For many of the interesting kinematic regions at both the LHC, and at higher energy colliders, there can be simultaneously large QCD corrections and large electroweak corrections. It is not clear a priori whether the QCD and EW corrections should be multiplied together or added. These two possibilities lead to cross sections of the schematic forms

$$\begin{aligned} \sigma_{add} &\sim \sigma_0 \left[1 + \mathcal{O}(\alpha_s) + \mathcal{O}(\alpha_{EW})\right], \\ \sigma_{mult} &\sim \sigma_0 \left[1 + \mathcal{O}(\alpha_s)\right] \times \left[1 + \mathcal{O}(\alpha_{EW})\right], \end{aligned} \tag{1.6}$$

where we have denoted the combinations as σ_{add} and σ_{mult}, and the Born-level cross section by σ_0. Expanding the product of brackets in σ_{mult} shows that these two prescriptions differ by terms of order $\mathcal{O}(\alpha_s\alpha_{EW})$. Only a complete calculation of these mixed corrections can determine whether either of these prescriptions provides an accurate description of the perturbative expansion. Even in current data, this ambiguity can result in significant uncertainties in the comparison of standard model predictions to the data. Only for the case of inclusive Higgs production have the relative $\mathcal{O}(\alpha_s\alpha_{EW})$ corrections been calculated [76], in a tractable parametric limit. Although this result suggests that the multiplicative combination is a good approximation for Higgs production, this conclusion is not necessarily applicable to other processes.

1.4.7.1 Importance of Sudakov logarithms for basic processes

Dijet production The inclusive production of two jets (dijets) allows for a detailed study of QCD at TeV energies. It is also the main background for searches of new heavy particles from Beyond Standard Model

(BSM) physics decaying into dijet signatures. Inclusive jet and dijet production has been analyzed by the ATLAS [12] and CMS [140] collaborations at $\sqrt{s} = 7$ and 8 TeV showing sensitivity to dijet invariant masses of up to 5 TeV and jet transverse momenta of up to 2 TeV at the LHC. As shown in Fig. 1-11, at the current level of experimental and theoretical accuracy, the SM is able to describe data well. However, the size of the EW correction is comparable to the experimental uncertainty for highest p_{T} bins, thus the dijet measurement at $\sqrt{s} = 8$ TeV has already started probing the "Sudakov zone".

The EW corrections to dijet production shown in Fig. 1-11b are taken from Ref. [77]. These corrections comprise electroweak contributions of $\mathcal{O}\left(\alpha_s\alpha, \alpha^2\right)$ to the LO QCD prediction as well as NLO corrections through the order $\alpha_s^2\alpha$. The tree-level contributions are of the same generic size as the loop corrections at $\sqrt{s} = 8$ TeV. The total correction to the integrated cross section is negligible, typically staying below the per-cent level. However, the Sudakov logarithms affect the tails of the distributions in the dijet invariant mass and in the transverse momenta of the two jets. The magnitude of the corrections at $\sqrt{s} = 8$ TeV and 14 TeV were found to be similar in Ref. [77]. Results from repeating the exact same calculation for $\sqrt{s} = 33$ TeV and 100 TeV are shown in Fig. 1-12 and Fig. 1-13, respectively. We find that the 1-loop virtual corrections are not so dependent on the collider energy, while the tree-level corrections decrease with $\sqrt{s}$. Their cancellation is less perfect, and as a result, the virtual negative corrections dominate in the kinematic tails at large $\sqrt{s}$. Since the kinematic reach will increase with increase in $\sqrt{s}$, these corrections will become progressively more important.

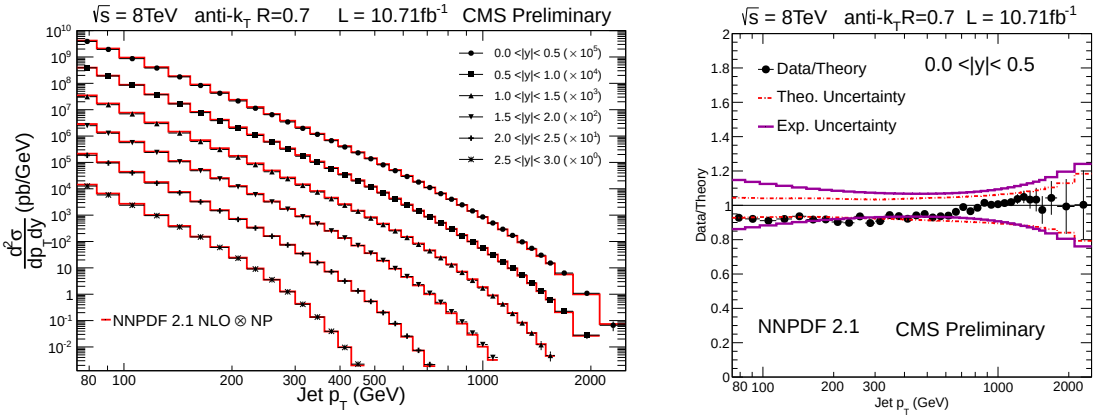

Figure 1-11. *Jet transverse momentum measured in 8 TeV pp collisions (top left) along with uncertainties (top right) from Ref. [140]. Also shown are the relative magnitude of electroweak corrections at pp collision energy of 8 TeV (bottom) taken from Ref. [77].*

Figure 1-12. *Dijet production: Differential distributions with respect to the dijet invariant mass M_{12} (top), the transverse momentum of the leading jet $k_{\mathrm{T},1}$ (middle) and the subleading jet $k_{\mathrm{T},2}$ (bottom) at the pp collision energy of 33 TeV. Left: absolute predictions; right: relative contributions δ.*

Figure 1-13. *Dijet production: Same distributions as in Fig. 1-12 for pp collision energy of 100 TeV.*

Inclusive vector boson production The production of a single electroweak boson is one of the basic hard-scattering processes at the LHC and constitutes major background for BSM searches like W'$\to \ell\nu$ and Z'$\to \ell\ell$ and important SM measurements like H$\to$ZZ$^* \to 4\ell$. Like in the diboson case, the virtual

corrections due to electroweak-boson exchanges can become quite significant. Since we are considering single electroweak-boson production, without additional radiation of soft or collinear W or Z bosons, the cross section will contain Sudakov logarithms that can be as large as 20% for boson $p_{\mathrm{T}} \sim 1$ TeV at the LHC. These effects need to be included for precise prediction of kinematic distribution in the region $p_{\mathrm{T}} \gg M_{\mathrm{V}}$. Inclusive W and Z spectra have been analyzed by the ATLAS [141] and CMS [138] collaborations at $\sqrt{s} = 8$ TeV showing sensitivity to invariant masses of up to 2 TeV and boson transverse momenta of up to 800 GeV. As shown in Fig. 1-14, at the current level of experimental and theoretical accuracy, the SM is able to describe data well. The current experimental uncertainty for invariant masses above 1 TeV is somewhat larger than the size of the EW corrections. The same measurements at 14 TeV will be sensitive to probing the Sudakov zone.

For above comparison we use Ref. [78] which provides computation of EW Sudakov effects in single W, Z, and γ production at large transverse momentum at $\sqrt{s} = 7$ TeV, with both QCD and electroweak effects included. Results from repeating the exact same calculation for $\sqrt{s} = 33$ TeV and 100 TeV are shown in Fig. 1-15. We find that the relative corrections are basically independent of $\sqrt{s}$, i.e., the corrections depend only on p_{T}, and not on $\sqrt{s}$. However, as the kinematic reach increases with increase in $\sqrt{s}$ these corrections will become progressively more important.

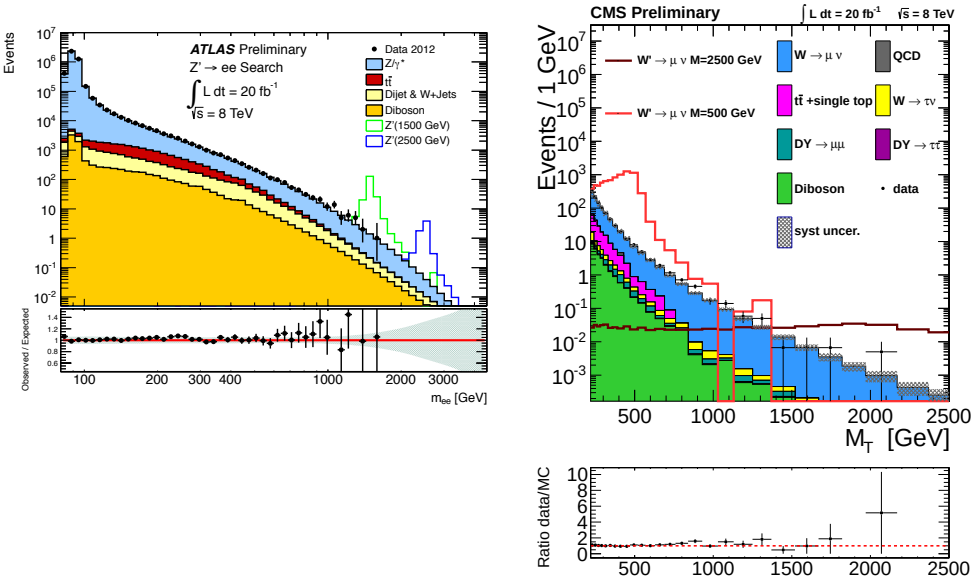

Figure 1-14. *(left) Observed dielectron invariant mass distribution in events containining two energetic electrons in 8 TeV pp collisions compared to the SM expectation. See Ref. [141] for details. (right) Observed transverse mass distribution of the muon + $\not{E}_{\mathrm{T}}$ system in events containing a high p_{T} muon and large $\not{E}_{\mathrm{T}}$ in 8 TeV pp collisions compared to the SM expectation. See Ref. [138] for details.*

Vector boson production in association with jets The production of a W or Z boson in association with jets has played a special role in collider physics. It was the dominant background to top-quark pair

production at the Tevatron. At the LHC it remains an important background for processes involving lepton, missing energy, and jets. Prominent examples are measurements of top quarks, Higgs bsoson, and multi-bososn production and BSM searches for supersymmetry signatures. Such measurements also permit stringent tests of the predictions of the Standard Model. Measurements of W and Z boson production in association with multiple jets have been made by the ATLAS [129, 130, 142] and CMS [134, 135, 139] collaborations at $\sqrt{s} = 7$ and 8 TeV showing sensitivity to boson and leading jet transverse momenta of up to about 500 GeV at the LHC. As shown in Fig. 1-16, at the current level of experimental and theoretical accuracy, the SM is able to describe data well. The current experimental uncertainty for highest p_{T} bins is somewhat larger than the size of the EW corrections. The same measurements at 14 TeV will be sensitive to probing the Sudakov zone.

The cross sections for W/Z + 1-jet, W/Z + 2-jet, W/Z + 3-jet, W + 4-jet, and W + 5-jet production are known at NLO QCD [131, 62]. The full NLO EW corrections for W + 1-jet production have been computed for the final state containing a charged lepton, a neutrino, and a hard jet [95]. The full NLO EW corrections for Z + 1-jet production have also been computed for the final state containing two charged leptons and a hard jet [96]. The overall magnitude of these corrections as a function of boson p_{T} is similar to the inclusive W/Z case. Results from repeating the exact same calculation as in Ref. [96] for Z + 1-jet events at $\sqrt{s} = 33$ TeV are listed in Tables. 1-4 and 1-5 as a function of the leading jet p_{T} and dilepton invariant mass, respectively. Results for $\sqrt{s} = 100$ TeV are listed in Tables. 1-6 and 1-7 respectively. We find that the relative corrections show very week dependence on $\sqrt{s}$ and depend mostly on jet (or boson) p_{T} and the invariant mass of the boson system. However, as the kinematic reach increases with increase in $\sqrt{s}$ these corrections will become progressively more important.

Vector-boson pair production Vector-boson pair production is among the most important SM benchmark processes at the LHC, because of its connection to the electroweak symmetry breaking, probe of Higgs boson production in $gg/q\bar{q} \to \mathrm{H} \to \mathrm{WW}^*$, ZZ^*, $\gamma\gamma$ processes, and probe of gauge boson self interactions. Diboson production can also help to gain a deeper understanding of the electroweak interaction in general, and to test the validity of the SM at highest energies.

Here we focus on WW production at large invariant masses or large W p_{T}, which is the kinematic regime of high interest and can have large EW corrections. This kinematic regime has recently been analyzed by the ATLAS [136] and CMS [137] collaborations at $\sqrt{s} = 8$ TeV showing sensitivity to invariant masses of up to 1 TeV and boson transverse momenta of up to 500 GeV. Comparing with the full one-loop EW corrections to on-shell WW production [28] we find that the size of the correction is comparable to the experimental uncertainty for highest kinematic end points. As noted in Ref. [28], the corrections due to photon-induced channels can be large at high enrgies, while radiation of additional massive vector bosons does not influence the results significantly. Results from repeating the exact same calculation for $\sqrt{s} = 33$ TeV and 100 TeV are shown in Fig. 1-18. We find that while the relative NLO EW corrections hardly depend on the collider energy, the relative photon-induced contributions are suppressed at to larger values of $\sqrt{s}$. As a result, the overall corrections show very little dependence on $\sqrt{s}$. However, like in the case of other processes described earlier, the EW corrections will progressively become more important with increase in $\sqrt{s}$ due to higher kinematic reach.

Summary We have presented a survey of the most abundant processes at LHC for sensitivity to electroweak corrections at various proton-proton collision energies relevant for LHC and future hadron colliders. We summarize our observations in Table 1-8. We find that for most processes the overall electroweak corrections do not change much with increase in collider energy. However, the corrections become more important at

$\mathrm{pp} \to l^+l^-$ jet $+ X$ at $\sqrt{s} = 33\,\mathrm{TeV}$

$p_{\mathrm{T,jet}}$/ GeV	$50 - \infty$	$100 - \infty$	$200 - \infty$	$400 - \infty$	$1000 - \infty$	$2000 - \infty$
$\sigma^{\mu=M_\mathrm{Z}}_{\mathrm{Born}}$/ pb	121.26(1)	33.737(4)	6.3314(7)	0.79429(9)	0.026920(2)	0.0010264(1)
$\sigma^{\mathrm{var}}_{\mathrm{Born}}$/ pb	120.70(1)	32.654(4)	5.6403(7)	0.60157(6)	0.014491(1)	0.00038663(4)
$\delta^{\mu=M_\mathrm{Z}}_{\mathrm{EW}}/\%$	−4.68(1)	−5.47(1)	−9.25(1)	−16.15(2)	−29.25(5)	−41.8(2)
$\delta^{\mathrm{rec},\mu=M_\mathrm{Z}}_{\mathrm{EW}}/\%$	−3.29(3)	−4.48(2)	−8.50(4)	−15.42(3)	−28.59(8)	−41.0(1)
$\delta^{\mathrm{var}}_{\mathrm{EW}}/\%$	−4.61(1)	−5.31(1)	−8.92(1)	−15.65(2)	−28.48(5)	−40.5(3)
$\delta^{\mathrm{rec,var}}_{\mathrm{EW}}/\%$	−3.16(3)	−4.42(4)	−8.12(2)	−14.89(2)	−27.62(5)	−39.9(1)
$\delta^{\mu=M_\mathrm{Z}}_{\mathrm{QCD}}/\%$	56.1(2)	78.7(1)	113.0(1)	160.5(1)	240.4(2)	330.6(3)
$\delta^{\mathrm{var}}_{\mathrm{QCD}}/\%$	54.0(1)	77.4(1)	117.3(1)	186.0(1)	347.2(2)	609.0(4)
$\delta^{\mu=M_\mathrm{Z}}_{\mathrm{QCD,veto}}/\%$	13.1(1)	23.3(1)	29.7(1)	27.5(1)	−2.8(1)	−42.2(1)
$\delta^{\mathrm{var}}_{\mathrm{QCD,veto}}/\%$	12.9(1)	25.6(2)	38.8(1)	49.8(1)	52.6(1)	54.0(1)
$\delta^{\mu=M_\mathrm{Z}}_{\gamma,\mathrm{Born}}/\%$	0.1377(4)	0.1647(4)	0.1960(5)	0.2442(7)	0.341(1)	0.457(1)
$\delta^{\mathrm{var}}_{\gamma,\mathrm{Born}}/\%$	0.1489(4)	0.1923(5)	0.2562(7)	0.371(1)	0.661(2)	1.095(3)
$\sigma^{\mathrm{var}}_{\mathrm{full,veto}}$/ pb/%	130.9(2)	39.36(6)	7.342(9)	0.8091(7)	0.01808(2)	0.000443(1)

Table 1-4. *Z + 1-jet production: Integrated cross sections for different cuts on the p_T of the leading jet (jet with highest p_T) at a proton-proton collider with $\sqrt{s} = 33$ TeV. The LO results are shown both for a variable and for a constant scale. The relative EW corrections δ_EW are given with and without lepton-photon recombination. The QCD corrections δ_QCD are presented for a fixed as well as a for variable scale and with or without employing a veto on a second hard jet. The EW corrections and the corrections due to photon-induced processes, δ_γ, are presented for the variable scale. Finally, the last row shows the full NLO cross section $\sigma^{\mathrm{var}}_{\mathrm{full,veto}}$. The error from the Monte Carlo integration for the last digit(s) is given in par enthesis as far as significant. See Ref. [96] for details.*

$\mathrm{pp} \to l^+l^-$ jet $+ X$ at $\sqrt{s} = 33\,\mathrm{TeV}$

M_{ll}/ GeV	$100 - \infty$	$200 - \infty$	$400 - \infty$	$1000 - \infty$	$2000 - \infty$	$4000 - \infty$
$\sigma^{\mu=M_Z}_{\mathrm{Born}}$/ pb	19.924(6)	1.6890(2)	0.28005(4)	0.022682(3)	0.0024968(4)	0.00015626(2)
$\sigma^{\mathrm{var}}_{\mathrm{Born}}$/ pb	19.849(6)	1.6482(2)	0.26618(4)	0.020604(3)	0.0021755(3)	0.00012945(2)
$\delta^{\mu=M_Z}_{\mathrm{EW}}$/%	−9.6(1)	−5.74(1)	−8.26(1)	−14.31(2)	−21.69(3)	−31.92(4)
$\delta^{\mathrm{rec},\mu=M_Z}_{\mathrm{EW}}$/%	−5.3(1)	−3.06(1)	−5.13(1)	−10.11(2)	−16.34(3)	−24.77(4)
$\delta^{\mathrm{var}}_{\mathrm{EW}}$/%	−9.46(8)	−5.69(1)	−8.14(1)	−14.18(2)	−21.56(3)	−31.88(6)
$\delta^{\mathrm{rec},\mathrm{var}}_{\mathrm{EW}}$/%	−5.05(7)	−2.94(1)	−4.93(1)	−9.93(2)	−16.14(3)	−24.75(6)
$\delta^{\mu=M_Z}_{\mathrm{QCD}}$/%	29.(1)	14.8(2)	−0.6(1)	−29.5(1)	−57.1(1)	−89.5(1)
$\delta^{\mathrm{var}}_{\mathrm{QCD}}$/%	27.9(6)	15.9(2)	2.2(1)	−23.0(1)	−46.6(1)	−74.8(1)
$\delta^{\mu=M_Z}_{\mathrm{QCD,veto}}$/%	5.0(6)	−8.9(2)	−25.5(1)	−54.9(1)	−82.4(1)	−115.3(1)
$\delta^{\mathrm{var}}_{\mathrm{QCD,veto}}$/%	6.1(4)	−7.2(2)	−20.8(2)	−45.8(1)	−69.8(1)	−98.1(1)
$\delta^{\mu=M_Z}_{\gamma,\mathrm{Born}}$/%	0.669(1)	2.097(5)	2.409(6)	2.168(6)	1.844(5)	1.610(3)
$\delta^{\mathrm{var}}_{\gamma,\mathrm{Born}}$/%	0.710(1)	2.298(5)	2.721(7)	2.510(7)	2.135(5)	1.822(3)
$\sigma^{\mathrm{var}}_{\mathrm{full,veto}}$/ pb/%	19.32(9)	1.473(4)	0.1965(6)	0.00877(2)	0.000234(3)	−0.0000365(2)

Table 1-5. *Z + 1-jet production: Integrated cross sections for different cuts on the dilepton invariant mass at a proton-proton collider with $\sqrt{s} = 33$ TeV. See aption of Table 1-4 and text for details.*

$\mathrm{pp} \to l^+l^-$ jet $+ X$ at $\sqrt{s} = 100\,\mathrm{TeV}$

$p_{\mathrm{T,jet}}$/ GeV	$100 - \infty$	$200 - \infty$	$400 - \infty$	$800 - \infty$	$2000 - \infty$	$4000 - \infty$
$\sigma^{\mu=M_Z}_{\mathrm{Born}}$/ pb	114.29(1)	23.772(3)	3.5452(4)	0.42003(4)	0.017238(1)	0.00094403(9)
$\sigma^{\mathrm{var}}_{\mathrm{Born}}$/ pb	118.30(1)	23.762(3)	3.1922(3)	0.31583(3)	0.0091290(9)	0.00035205(3)
$\delta^{\mu=M_Z}_{\mathrm{EW}}$/%	−5.62(1)	−9.57(1)	−16.86(2)	−27.11(8)	−43.5(1)	−58.8(1)
$\delta^{\mathrm{rec},\mu=M_Z}_{\mathrm{EW}}$/%	−4.65(3)	−8.72(2)	−16.08(2)	−26.29(4)	−43.15(7)	−58.5(2)
$\delta^{\mathrm{var}}_{\mathrm{EW}}$/%	−5.50(1)	−9.29(1)	−16.38(3)	−26.36(4)	−43.2(2)	−57.5(1)
$\delta^{\mathrm{rec},\mathrm{var}}_{\mathrm{EW}}$/%	−4.48(2)	−8.52(2)	−15.62(2)	−25.64(4)	−42.21(7)	−56.8(1)
$\delta^{\mu=M_Z}_{\mathrm{QCD}}$/%	97.4(2)	146.0(1)	215.2(2)	288.7(2)	378.0(3)	472.6(5)
$\delta^{\mathrm{var}}_{\mathrm{QCD}}$/%	85.4(2)	130.0(2)	201.7(1)	298.8(2)	487.9(3)	769.0(7)
$\delta^{\mu=M_Z}_{\mathrm{QCD,veto}}$/%	35.7(2)	54.2(1)	66.7(1)	61.3(1)	13.2(2)	−43.1(1)
$\delta^{\mathrm{var}}_{\mathrm{QCD,veto}}$/%	29.6(2)	47.4(1)	65.5(1)	76.4(3)	65.6(2)	51.5(1)
$\delta^{\mu=M_Z}_{\gamma,\mathrm{Born}}$/%	0.1218(3)	0.1400(4)	0.1681(5)	0.2114(7)	0.291(1)	0.382(1)
$\delta^{\mathrm{var}}_{\gamma,\mathrm{Born}}$/%	0.1407(3)	0.1799(5)	0.2482(7)	0.365(1)	0.630(2)	1.006(5)
$\sigma^{\mathrm{var}}_{\mathrm{full,veto}}$/ pb/%	147.0(2)	32.86(4)	4.767(4)	0.475(1)	0.01124(2)	0.0003343(7)

Table 1-6. *Z + 1-jet production: Integrated cross sections for different cuts on the p_{T} of the leading jet at a proton-proton collider with $\sqrt{s} = 100$ TeV. See aption of Table 1-4 and text for details.*

$\mathrm{pp} \to l^+l^-$ jet $+ X$ at $\sqrt{s} = 100\,\mathrm{TeV}$

M_{ll}/ GeV	$100-\infty$	$200-\infty$	$400-\infty$	$1000-\infty$	$2000-\infty$	$4000-\infty$
$\sigma_{\mathrm{Born}}^{\mu=M_Z}$/ pb	60.70(2)	5.3194(9)	0.9142(1)	0.08462(1)	0.012762(2)	0.0016229(2)
$\sigma_{\mathrm{Born}}^{\mathrm{var}}$/ pb	61.76(2)	5.3548(9)	0.9016(1)	0.07980(1)	0.011500(2)	0.0013850(2)
$\delta_{\mathrm{EW}}^{\mu=M_Z}$/%	−9.4(1)	−5.85(1)	−8.41(1)	−14.28(2)	−21.05(3)	−29.97(5)
$\delta_{\mathrm{EW}}^{\mathrm{rec},\mu=M_Z}$/%	−5.0(1)	−3.23(1)	−5.29(1)	−10.42(3)	−16.42(3)	−24.34(5)
$\delta_{\mathrm{EW}}^{\mathrm{var}}$/%	−9.5(2)	−5.76(1)	−8.31(1)	−14.08(2)	−20.85(3)	−29.87(5)
$\delta_{\mathrm{EW}}^{\mathrm{rec,var}}$/%	−5.2(2)	−3.07(1)	−5.15(2)	−10.11(2)	−16.22(4)	−24.09(5)
$\delta_{\mathrm{QCD}}^{\mu=M_Z}$/%	36.(4)	20.8(3)	7.3(2)	−18.1(1)	−43.3(1)	−73.7(1)
$\delta_{\mathrm{QCD}}^{\mathrm{var}}$/%	29.3(9)	18.4(3)	6.0(1)	−16.3(1)	−37.4(1)	−63.3(1)
$\delta_{\mathrm{QCD,veto}}^{\mu=M_Z}$/%	5.0(9)	−7.0(2)	−21.2(2)	−46.8(1)	−71.8(1)	−102.1(1)
$\delta_{\mathrm{QCD,veto}}^{\mathrm{var}}$/%	3.8(7)	−7.4(3)	−19.6(2)	−41.7(1)	−63.1(1)	−88.5(2)
$\delta_{\gamma,\mathrm{Born}}^{\mu=M_Z}$/%	0.532(1)	1.679(4)	2.019(6)	1.988(6)	1.792(6)	1.511(4)
$\delta_{\gamma,\mathrm{Born}}^{\mathrm{var}}$/%	0.568(1)	1.871(4)	2.363(7)	2.464(7)	2.259(7)	1.901(5)
$\sigma_{\mathrm{full,veto}}^{\mathrm{var}}$/ pb/%	58.6(4)	4.75(1)	0.672(1)	0.0373(1)	0.00211(2)	−0.000228(3)

Table 1-7. *Z + 1-jet production: Integrated cross sections for different cuts on the dilepton invariant mass at a proton-proton collider with $\sqrt{s} = 100$ TeV. See aption of Table 1-4 and text for details.*

high collider energies simply because of increase in kinematic reach at high $\sqrt{s}$, where the corrections are inherently large.

Table 1-8. *Are we in the Sudakov zone yet?*

Process	$\sqrt{s} = 8$ TeV	$\sqrt{s} = 14$ TeV	$\sqrt{s} = 33, 100$ TeV
Inclusive jet, dijet	Yes	Yes	Yes
Inclusive W/Z tail	$\sim$ Yes	Yes	Yes
Wγ, Zγ tail ($\ell\nu\gamma, \ell\ell\gamma$)	No	$\sim$ Yes	Yes
W/Z+jets tail	$\sim$ Yes	Yes	Yes
WW leptonic	Close	$\sim$ Yes	Yes
WZ, ZZ leptonic	No	No	Yes
WW, WZ, ZZ semileptonic	$\sim$ Yes	Yes	Yes

1.4.7.2 Interplay of electroweak and QCD corrections in Drell-Yan production

The effects of electroweak Sudakov logarithms on more differential quantities, and their interplay with higher-order QCD corrections, are studied next for the example case of lepton-pair production via the Drell-Yan mechanism at a 33 TeV pp collider. The results shown are obtained with the numerical program FEWZ [114, 115, 116], which additively combines higher-order QCD and electroweak corrections. MSTW PDFs at the appropriate order in QCD perturbation theory are used. Shown first in Fig. 1-19 is the lepton-pair invariant mass distribution, with minimal acceptance cuts imposed on the transverse momenta and

pseudorapidities of the leptons. The shift due to NLO QCD corrections alone is shown, as is the result of combining the full NLO electroweak correction with the QCD one. Both shifts are normalized to the leading-order prediction. Over a broad range of invariant masses, the QCD corrections increase the cross section by $20 - 30\%$. The electroweak corrections grow in importance with invariant mass, and lead to a decrease in the cross section. The electroweak corrections begin to overtake the QCD ones at $M_{ll} \approx 5$ TeV, and the reduction in the cross section from the combined corrections reaches 30% at invariant masses of 15 TeV.

The shifts induced by the combined QCD and electroweak corrections on the lepton differential distributions are considered next. The cross section is first divided into the following invariant mass bins: $M_{ll} \in [500\,\text{GeV}, 1\,\text{TeV}]$, $M_{ll} \in [1\,\text{TeV}, 5\,\text{TeV}]$, and $M_{ll} \in [5\,\text{TeV}, 20\,\text{TeV}]$. The lepton transverse momenta and pseudorapidity distributions in each bin are then studied. The results are shown in Figs. 1-20, 1-21, and 1-22. The QCD and electroweak corrections have the same shape as a function of lepton p_T. The dips appearing in the corrections at half the lower bin edge, and the rise at the upper bin edge, are artifacts of the Jacobian peaks present in the leading-order result. An interesting feature emerges in the lepton η distributions at higher invariant masses. The electroweak corrections act more strongly for central pseudorapidities, leading to a dip in the combined corrections that is quite large for the highest invariant mass bin.

1.4.7.3 Electroweak corrections to $Z + 2$ and $Z + 3$ jets hadroproduction in the Sudakov zone

Important searches for new physics (NP) beyond the Standard Model (SM) at present and future proton-proton (pp) colliders are based on the analysis of events with jets and missing transverse momentum ($\not{p}_T$).

The main SM backgrounds to the above signature are given by the production of weak bosons accompanied by jets ($W/Z + n$ jets), pure QCD multiple jet events and $t\bar{t}$ production. Among these processes only $Z + n$ jets (in particular with $Z \to \nu\bar{\nu}$) constitutes an irreducible background, particularly relevant for final states with 2 and 3 jets.

The one-loop Sudakov logs are naturally included in any complete calculation of NLO EW radiative corrections to a given process. Up to now, these calculations are available for a limited class of processes, see for instance [90, 91, 92, 93, 94, 95, 96, 97, 77, 98] in particular of the kind $2 \to 2$ or $2 \to 3$ final state particles. On the other hand, by virtue of their universality, the Sudakov logarithmic contributions can be accounted for by means of process-independent methods, as shown in Ref. [99, 100, 101, 102, 103, 104, 105, 106, 107, 108, 109]. In particular, Denner and Pozzorini presented a method to single out DL and SL Sudakov contributions, as detailed in [104, 105]. The generality of this algorithm has been recently combined [110] with the leading order matrix element event generator `ALPGEN v2.1.4` [111], to obtain a tool able to calculate NLO EW Sudakov corrections to processes involving multijet final states. Phenomenological results have been presented in Ref. [110] for the production processes $Z(\to \nu\bar{\nu}) + 2(3)$ jets in pp collisions at $\sqrt{s} = 7, 14$ TeV.

The considered processes are, at the leading order $\alpha_s^{njets}\alpha$, of neutral current type, so the EW contributions can be separated in purely weak corrections (which contain the Sudakov logs and are the subject of the present contribution) and QED corrections. The latter can be treated separately together with their real counterpart and, for sufficiently inclusive event selections, they give rise to rather moderate corrections.

In this section, the focus is on the virtual EW Sudakov corrections to $Z + 2$ and $Z + 3$ jets hadroproduction, studying their scaling with the center of mass (c.m.) energy of proton-proton collisions from 14 TeV to 33 and 100 TeV. The event selections and considered observables are those of Ref. [110]. The parameters and PDF setting are the `ALPGEN` defaults. In particular, for $Z + 2$ jets, we consider the observable/cuts presently adopted by ATLAS [112], namely

$$m_{\text{eff}} > 1 \text{ TeV} \qquad \not{E}_T/m_{\text{eff}} > 0.3$$

$$
\begin{aligned}
&p_T^{j_1} > 130 \text{ GeV} \qquad p_T^{j_2} > 40 \text{ GeV} \quad |\eta_j| < 2.8 \\
&\Delta\phi(\vec{p}_T^{\,j},\vec{\not\!\!H}_T) > 0.4 \quad \Delta R_{(j_1,j_2)} > 0.4
\end{aligned}
\tag{1.7}
$$

where j_1 and j_2 are the leading and next-to-leading p_T jets.

For the $Z + 3$ jets final state we consider the observables/cuts used by CMS [113, 133], namely

$$
\begin{aligned}
&H_T > 500 \text{ GeV} \qquad |\vec{\not\!\!H}_T| > 200 \text{ GeV} \\
&p_T^j > 50 \text{ GeV} \qquad |\eta_j| < 2.5 \quad \Delta R_{(j_i,j_k)} > 0.5 \\
&\Delta\phi(\vec{p}_T^{\,j_1,j_2},\vec{\not\!\!H}_T) > 0.5 \qquad \Delta\phi(\vec{p}_T^{\,j_3},\vec{\not\!\!H}_T) > 0.3\,,
\end{aligned}
\tag{1.8}
$$

where $H_T = \sum_i p_{T\,i}$ and $\vec{\not\!\!H}_T = -\sum_i \vec{p}_{t\,i}$.

In Ref. [110] it has been shown that Sudakov virtual corrections to $Z + 2$ and $Z + 3$ jets production are negative and can be as large as about -40% at $\sqrt{s} = 7, 14$ TeV. Here we extend that analysis to c.m. energies of future hadronic colliders, namely 33 and 100 TeV. For the sake of reference, we report here some partial results from Ref. [110] corresponding to the c.m. energy of 14 TeV. In Figs. 1-23 and 1-24 we show the effect of the Sudakov logs on the effective mass distribution in the process $Z + 2$ jets according to the event selection of Eq. (1.7). All plots start from $m_{\text{eff}} = 1$ TeV and have different upper limits: 5 TeV for $\sqrt{s} = 14$ TeV, 10 TeV for $\sqrt{s} = 33$ TeV and 18 TeV for $\sqrt{s} = 100$ TeV. The upper panels display the effective mass distribution at LO (blue, solid) and including the approximate NLO virtual corrections (red, dotted) due to weak bosons in the Sudakov zone as calculated with `ALPGEN`, according to Ref. [110], respectively. The lower panels show the relative corrections due to virtual weak corrections. As can be seen, the negative correction due to Sudakov logs is of the order of some tens of per cent, raising to about 40% (60%, 80%) in the extreme regions at $\sqrt{s} = 14$ (33, 100) TeV, respectively. As can be naively expected, for a given bin of the m_{eff} distribution, the relative EW corrections is practically the same, independently of the collider c.m. energy. It is interesting to study whether and how the effects on the m_{eff} distribution change when adopting acceptance cuts scaled with the c.m. energy w.r.t. the case $\sqrt{s} = 14$ TeV (for simplicity the geometrical acceptance cuts are kept fixed). Figure 1-25 shows the predictions for

$$
\begin{aligned}
&m_{\text{eff}} > 2(7) \text{ TeV}\,, \ (\sqrt{s} = 33(100) \text{ TeV})\,, \\
&p_T^{j_1} > 260(910) \text{ GeV}\,, \ (\sqrt{s} = 33(100) \text{ TeV})\,, \\
&p_T^{j_2} > 80(280) \text{ GeV}, \ (\sqrt{s} = 33(100) \text{ TeV})\,,
\end{aligned}
$$

with the rest of the cuts unchanged w.r.t. Eq. (1.7). The effects of the tighter acceptance cuts are very mild, the leading effect being given by the m_{eff} cut.

In Figs. 1-26 and 1-27 we show the effect of the Sudakov logs on the observable $|\vec{\not\!\!H}_T|$ in the process $Z + 3$ jets according to the event selection of Eq. (1.8). All plots start from $|\vec{\not\!\!H}_T| = 0.2$ TeV and have different upper limits: 2.2 TeV for $\sqrt{s} = 14$ TeV, 4 TeV for $\sqrt{s} = 33$ TeV and 6 TeV for $\sqrt{s} = 100$ TeV. As for the $Z + 2$ jets effective mass distributions, the effect of NLO weak corrections on $|\vec{\not\!\!H}_T|$ is large and negative, raising to about 40% (60%, 70%) in the extreme regions at $\sqrt{s} = 14$ (33, 100) TeV, respectively. For a chosen $|\vec{\not\!\!H}_T|$ bin, the relative effects of the corrections are quite insensitive to the change of the collider energy and of the acceptance cuts. Figure 1-28 shows the $|\vec{\not\!\!H}_T|$ with scaled acceptance cuts:

$$
\begin{aligned}
&H_T > 1(3.5) \text{ TeV}\,, \ (\sqrt{s} = 33(100) \text{ TeV}) \\
&|\vec{\not\!\!H}_T| > 0.4(1.4) \text{ TeV}\,, \ (\sqrt{s} = 33(100) \text{ TeV}) \\
&p_T^j > 100(350) \text{ GeV}\,, \ (\sqrt{s} = 33(100) \text{ TeV})\,,
\end{aligned}
\tag{1.9}
$$

with the rest of the cuts unchanged w.r.t. Eq. (1.8). The changes in slope in the $|\vec{\not\!\!H}_T|$ distributions are due

to the presence of the cuts on the variable H_T.

To summarize, we computed the NLO EW Sudakov corrections to $Z+n$ jets, $n = 2, 3$, for two key observables, m_{eff} and $|\vec{\not{H}}_T|$, used in NP searches at the LHC. In particular we studied the behavior of the corrections as a function of the different collider c.m. energy, up to 100 TeV. The relative corrections do not show sensitivity to the collider energy, they are negative and become very large (more than 50% in absolute value) for extreme kinematically accessible values of the observables. With such large negative effects, also the possible compensation of real heavy gauge boson radiation and the higher-order contributions (beyond one-loop) should be investigated.

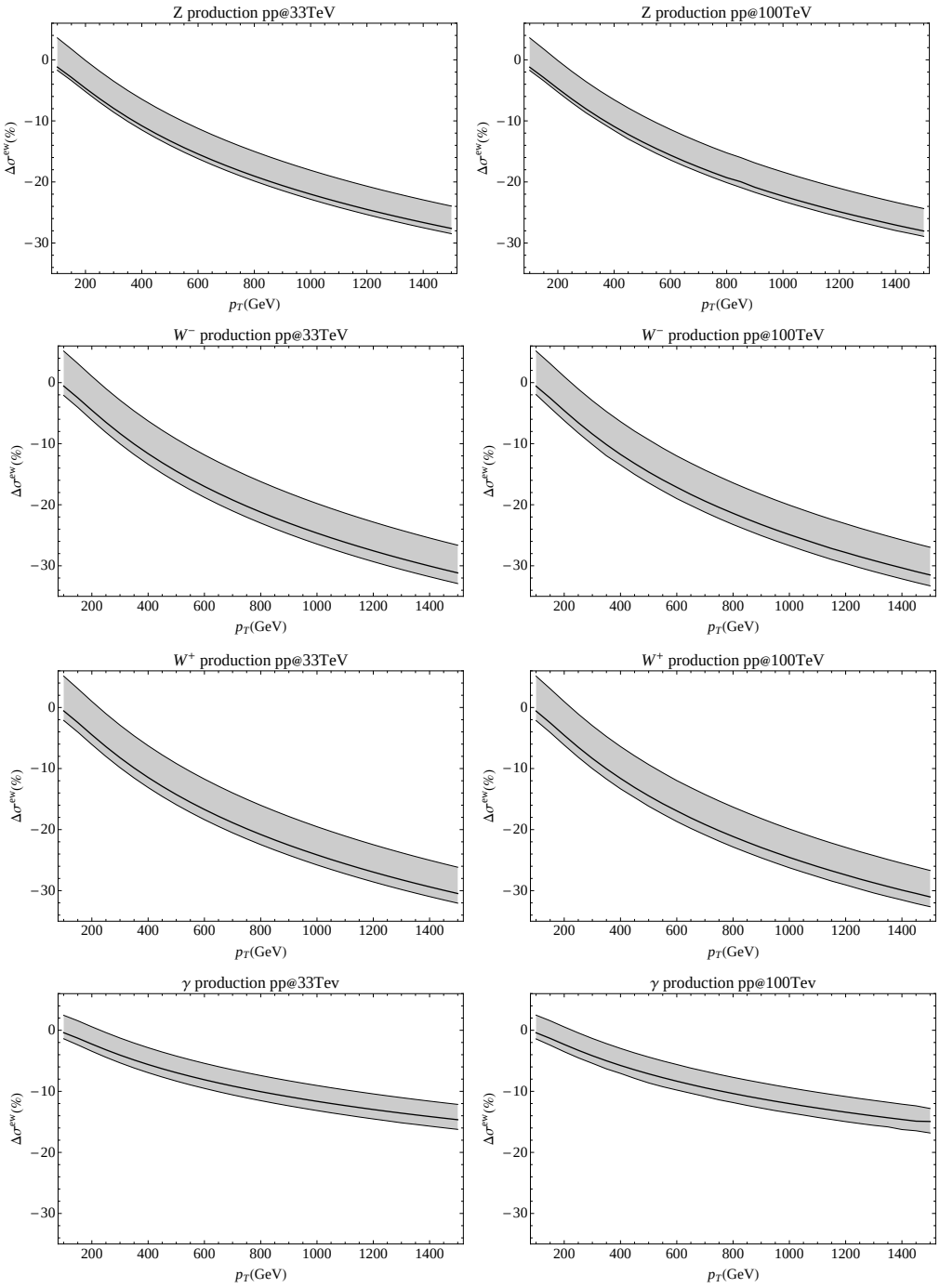

Figure 1-15. *Inclusive vector boson production: Relative contribution from electroweak corrections as a function of the vector boson transverse momentum for Z (row 1), W^- (row 2), W^+ (row 3), and γ (row 4). Left: at the pp collision energy of 33 TeV; right: at 100 TeV.*

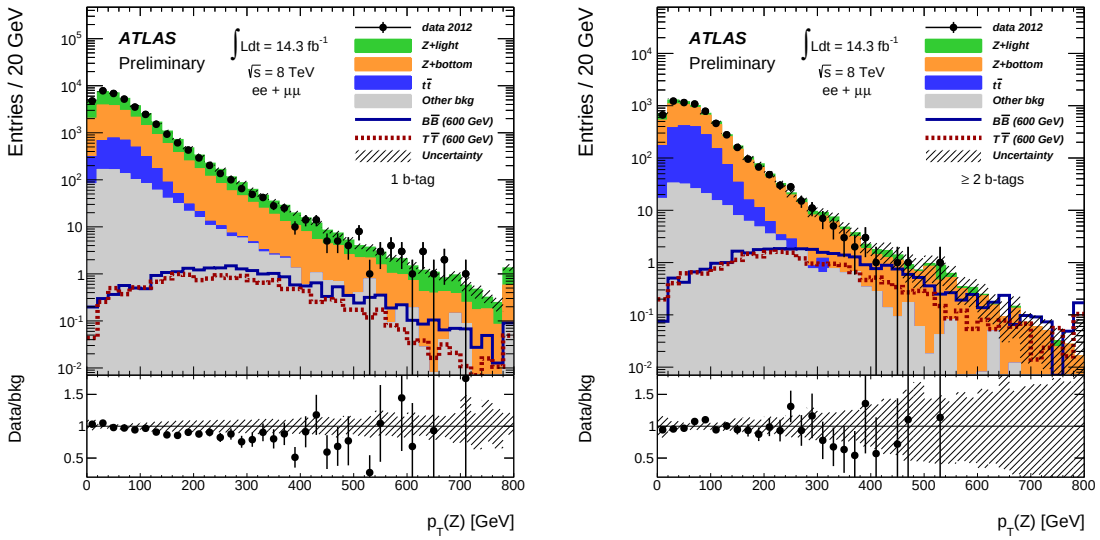

Figure 1-16. *The observed Z boson transverse momentum distribution in events containing at least two jets at $\sqrt{s} = 8$ TeV. (left) Exactly one jet is b-tagged. (right) at least two jets are b-tagged. For details see Ref. [142].*

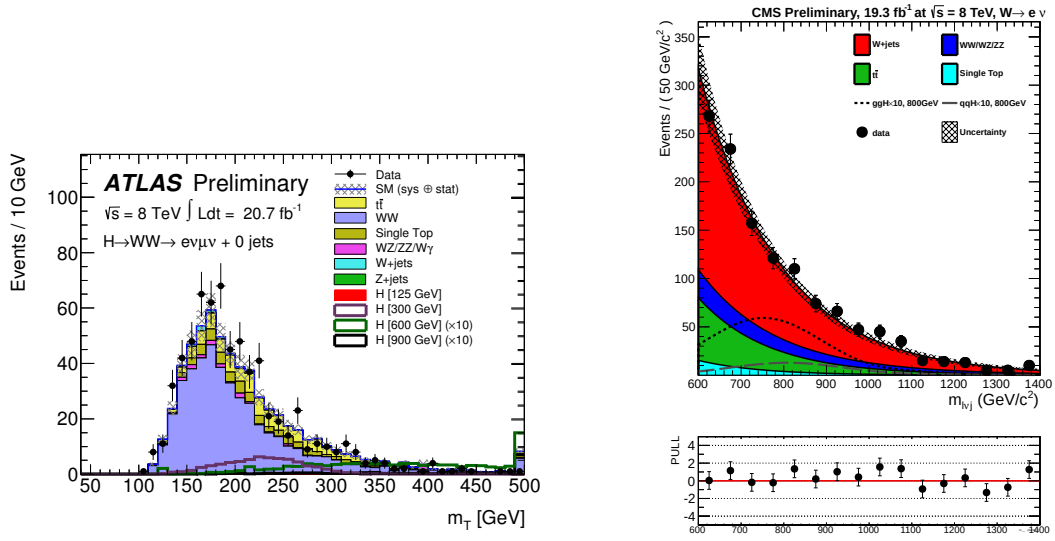

Figure 1-17. *(left) Observed transverse mass distributions of the WW system in the fully leptonic decay mode electron+muon+$\not{E}_{\mathrm{T}}$ and no jet activity at $\sqrt{s} = 8$ TeV. For details see Ref. [136]. (b) Observed invariant mass distribution of the WW candidates at $\sqrt{s} = 8$ TeV in the semi-leptonic decay mode where one W boson decays leptonically to $e\nu$ and the other W boson decays at high transverse momentum to $q\bar{q}$ giving rise to a single merged jet. For details see Ref. [137].*

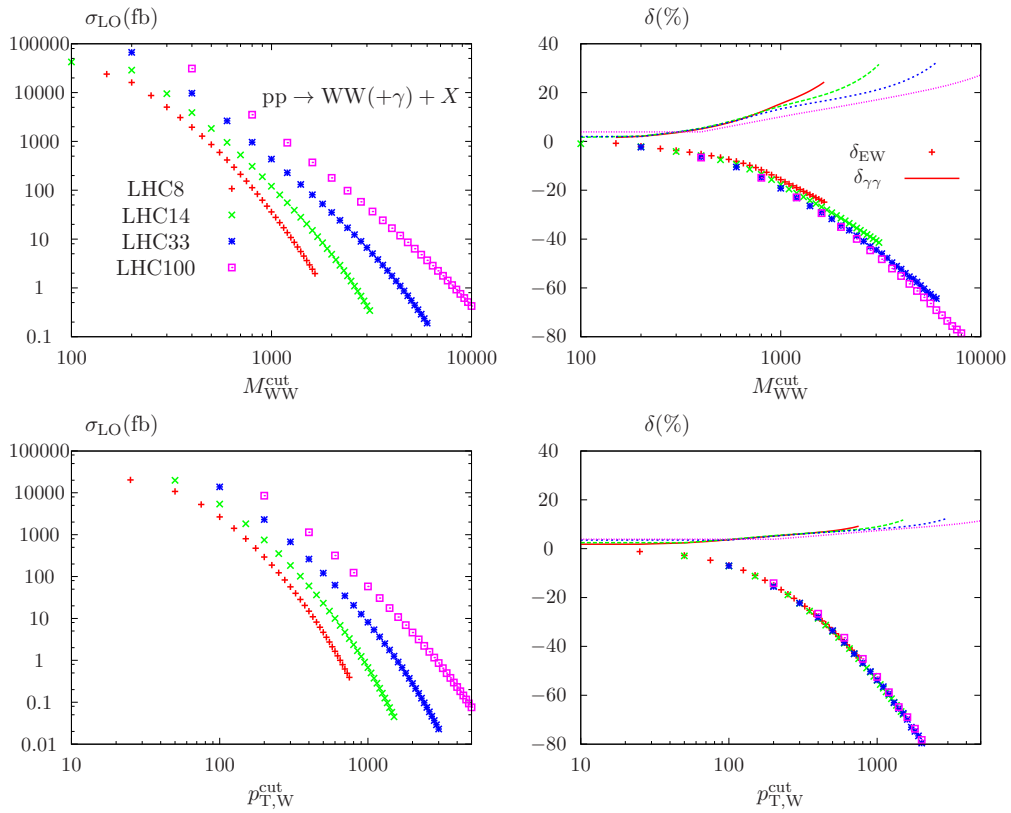

Figure 1-18. *WW production: Total cross sections for W-pair production for different cuts on WW invariant mass (top row) and W transverse momentum (bottom row), evaluated at pp collision energies of 8, 14, 33, and 100 TeV. Left: absolute predictions; right: relative contributions.*

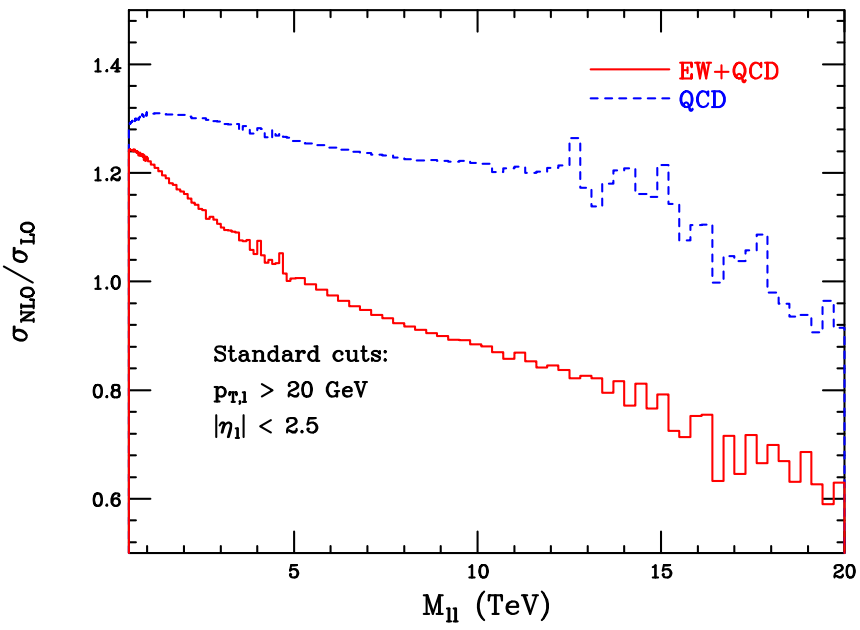

Figure 1-19. *QCD corrections and combined electroweak-QCD corrections to lepton-pair production as a function of the lepton-pair invariant mass, at a 33 TeV pp collider.*

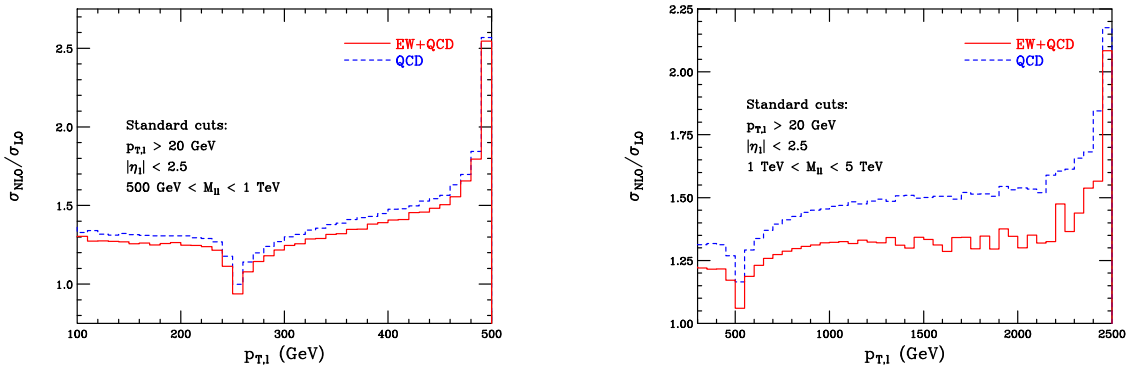

Figure 1-20. *QCD corrections and combined electroweak-QCD corrections to lepton-pair production as a function of the lepton transverse momentum, at a 33 TeV pp collider. Results for two bins of lepton-pair invariant mass, $M_{ll} \in [500\,\text{GeV}, 1\,\text{TeV}]$, and $M_{ll} \in [1\,\text{TeV}, 5\,\text{TeV}]$, are shown.*

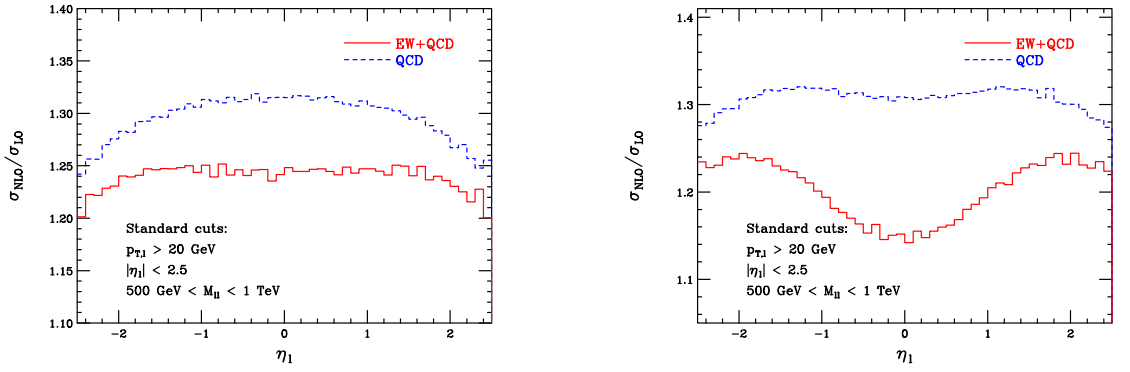

Figure 1-21. *QCD corrections and combined electroweak-QCD corrections to lepton-pair production as a function of the lepton pseudorapidity, at a 33 TeV pp collider. Results for two bins of lepton-pair invariant mass $M_{ll} \in [500\,\text{GeV}, 1\,\text{TeV}]$, and $M_{ll} \in [1\,\text{TeV}, 5\,\text{TeV}]$, are shown.*

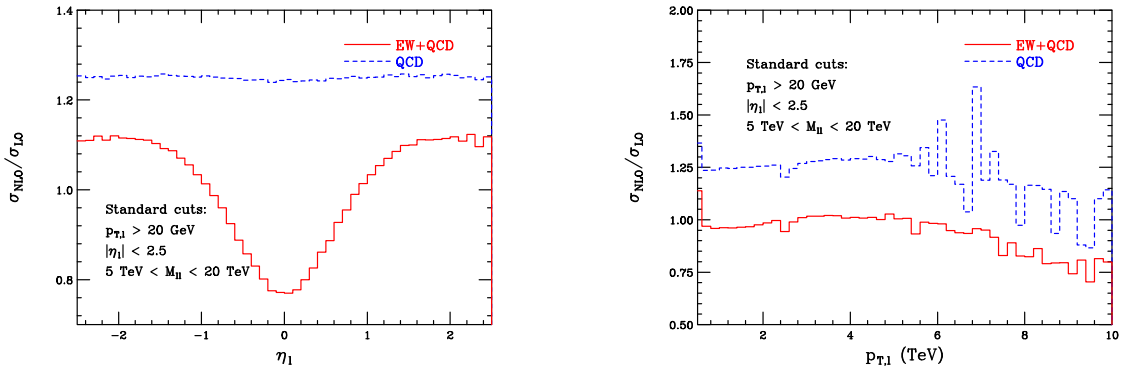

Figure 1-22. *QCD corrections and combined electroweak-QCD corrections to lepton-pair production as a function of the lepton pseudorapidity and transverse momentum, at a 33 TeV pp collider. Results for the bin of lepton-pair invariant mass $M_{ll} \in [5\,\text{TeV}, 20\,\text{TeV}]$ are shown*

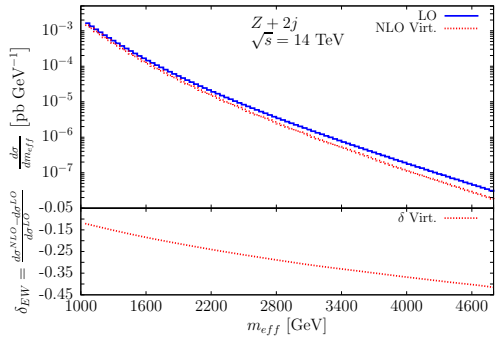

Figure 1-23. *$Z + 2$ jets: ATLAS m_{eff} and EW correction at $\sqrt{s} = 14$ TeV*

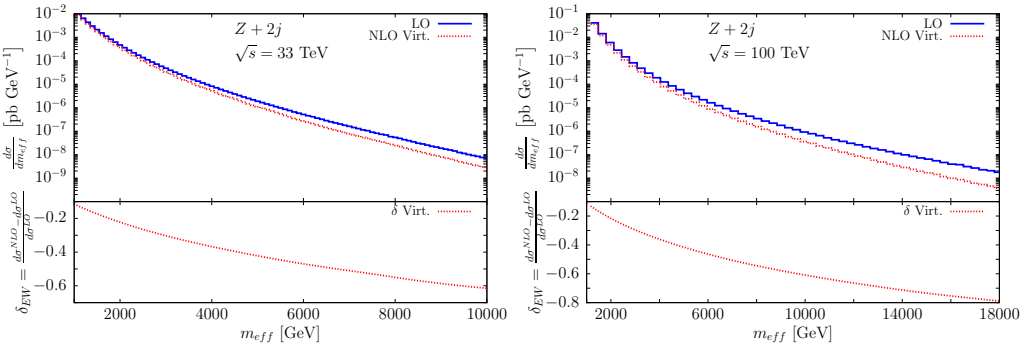

Figure 1-24. *The same as Fig. 1-23 at $\sqrt{s} = 33, 100$ TeV.*

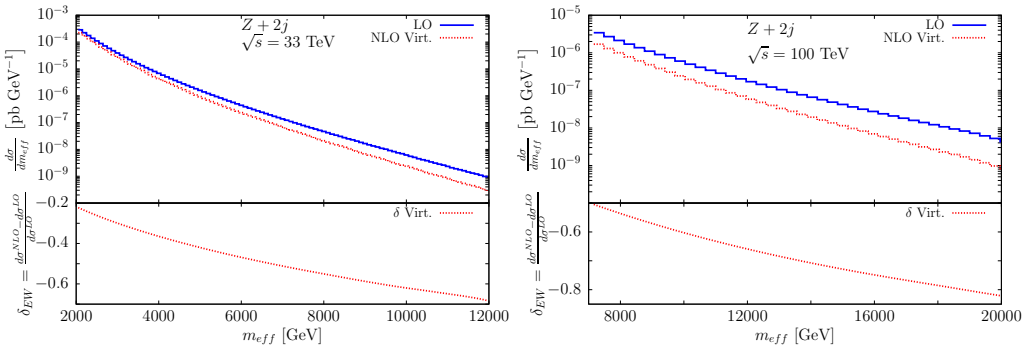

Figure 1-25. *The same as Fig. 1-24 with rescaled cuts, as described in the text.*

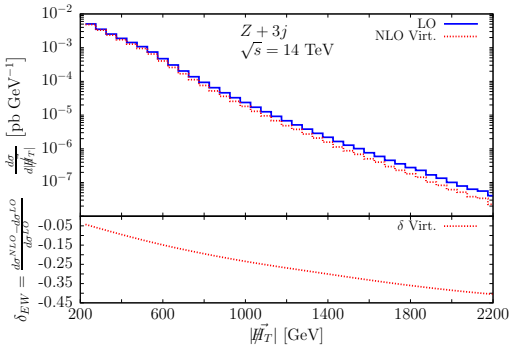

Figure 1-26. *$Z + 3$ jets: CMS $|\vec{\not{H}}_T|$ and EW correction at $\sqrt{s} = 14$ TeV.*

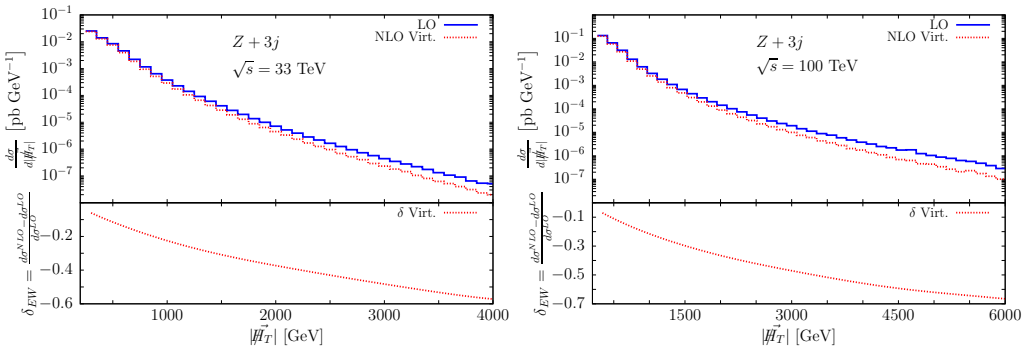

Figure 1-27. *The same as Fig. 1-26 at $\sqrt{s} = 33, 100$ TeV.*

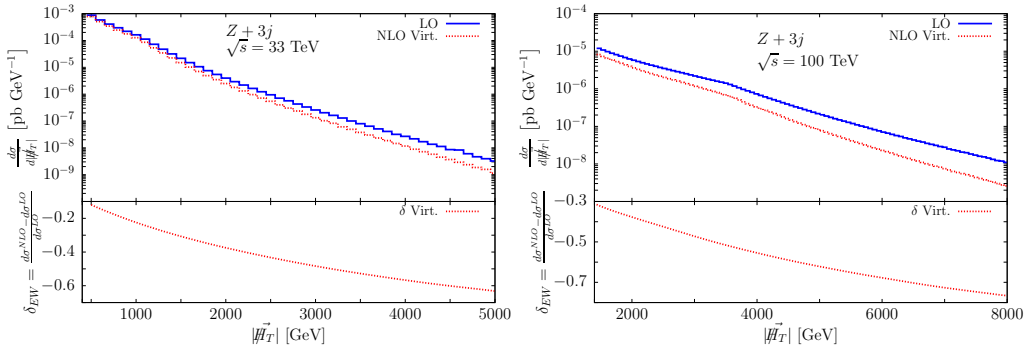

Figure 1-28. *The same as Fig. 1-27 with rescaled cuts, as described in the text.*

1.5 Jet vetoes and exclusive jet binning

1.5.1 Higgs production in gluon fusion

The discovery of the Higgs boson by the ATLAS and CMS collaborations has dominated the field of high energy physics during the past year. A large component of the future worldwide effort in particle physics will be devoted to measuring the properties of this state in order to determine the underlying theory from which it arises. Theoretical uncertainties from missing higher-order corrections are quickly becoming a limiting factor in this program. In the W^+W^- final state, the theoretical uncertainties are already a dominant systematic error [79, 132]. The reasons for this are two-fold. The perturbative expansion for inclusive Higgs boson production is slowly convergent, and indeed even corrections beyond NNLO change the prediction in a significant way, as described in Section 1.4.5 of this report. In addition, and most importantly for this Section, significant cuts are imposed on the phase space of the hadronic radiation produced in association with the Higgs. This is required because the background composition to this signal changes as a function of jet multiplicity. In the zero-jet bin the background is dominated by continuum WW production, while in the one-jet and two-jet bins, top-pair production becomes increasingly important. The optimization of this search requires cuts dependent on the number of jets observed, and therefore also on theoretical predictions for exclusive jet multiplicities.

The prediction of cross sections in bins of exclusive jet multiplicity poses an interesting theoretical challenge. The distribution for an observable τ in QCD perturbation theory has the structure shown in Fig. 1-29. This form of the distribution follows from the presence of Sudakov double logarithms, $\alpha_s/\pi \times \ln^2(Q/\tau_{cut})$,

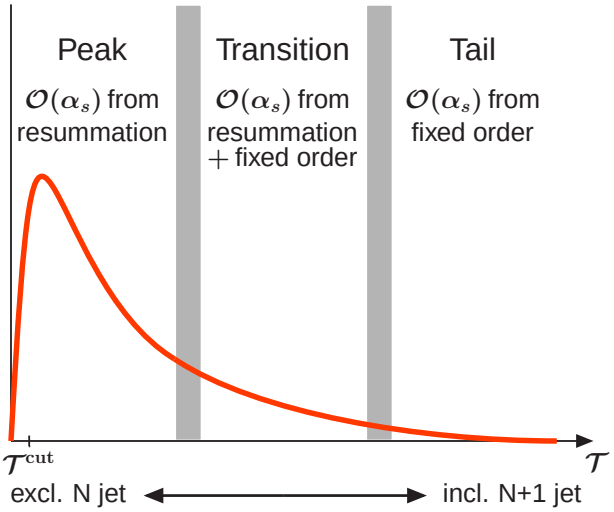

Figure 1-29. *Generic distribution for a variable τ obtained in QCD perturbation theory, taken from Ref. [80].*

appearing in the perturbative expansion for the cross section, where Q denotes the hard scale of the process such as the partonic center-of-momentum scattering energy, and τ_{cut} denotes some experimental constraint τ. When τ is relatively unconstrained and $\tau_{cut} \sim Q$ as in the tail region of Fig. 1-29, these logarithms are of order unity, and fixed-order QCD perturbation theory can be applied to predict the distribution. When $\tau_{cut} \ll Q$ in the peak region, the Sudakov logarithms overwhelm the α_s suppression, and the perturbative

expansion must be resummed to all orders to ensure that the distribution does not diverge as $\tau_{cut} \to 0$. However, techniques exist to perform this resummation, and the higher-order corrections in fixed-order perturbation theory give only small corrections in the peak region. The transition region is the theoretically most intricate region to predict. The logarithms are large enough that resummation must be performed, but not so large that the fixed-order corrections are negligible. Progress on both resummation and fixed-order calculations are needed to accurately describe such observables. Higgs production at the LHC in exclusive jet bins is an example of an observable in the transition region. For Higgs plus jets observables, $Q \sim m_H$ and $\tau_{cut} \sim p_T^{cut} = 25 - 30\,\text{GeV}$, where p_T^{cut} denotes the transverse momentum cut used to define a jet. Both higher-order corrections and resummation are needed to accurately predict the rates and distributions for Higgs plus jets. And since the hard scale Q grows with the partonic scattering energy, the high-p_T jet region accessible at potential future 33 TeV and 100 TeV colliders will potentially exhibit quite different behavior in QCD perturbation theory.

We begin with a discussion of the NNLO QCD calculation for Higgs plus one-or-more jets, for which initial results for the gluon channel have recently been reported [30], and attempt to provide questions and guidance for phenomenological studies at future colliders when the full result is available. We note that the cross section for inclusive Higgs plus one-or-more jets enters the prediction for the exclusive one-jet bin through the relation $\sigma_1 = \sigma_{\geq 1} - \sigma_{\geq 2}$, where the subscript denote the number of final-state jets produced in addition to the Higgs. We show the hadronic cross section for the production of the Higgs boson in association with one or more jets at the 8 TeV LHC through NNLO in perturbative QCD. Jets are reconstructed using the $k_\perp$-algorithm with $R = 0.5$ and $p_T^{cut} = 30$ GeV. The Higgs mass is taken to be $m_H = 125$ GeV, and NNPDF parton distributions are used [10]. The central renormalization and factorization scales are set to be $\mu_R = \mu_F = m_H$.

In Fig. 1-30 we show the partonic cross section for $gg \to H + j$ multiplied by the gluon luminosity through NNLO in perturbative QCD:

$$\beta \frac{\mathrm{d}\sigma_{\rm had}}{\mathrm{d}\sqrt{s}} = \beta \frac{\mathrm{d}\sigma(s, \alpha_s, \mu_R, \mu_F)}{d\sqrt{s}} \times \mathcal{L}(\frac{s}{s_{\rm had}}, \mu_F), \tag{1.10}$$

where β measures the distance from the partonic threshold,

$$\beta = \sqrt{1 - \frac{E_{th}^2}{s}}, \qquad E_{th} = \sqrt{m_H^2 + p_{\perp,j}^2} + p_{\perp,j} \approx 158.55 \text{ GeV}. \tag{1.11}$$

It follows from Fig. 1-30 that NNLO QCD corrections are significant in the region $\sqrt{s} < 500$ GeV. In particular, close to partonic threshold $\sqrt{s} \sim E_{th}$, radiative corrections are enhanced by threshold logarithms $\ln \beta$ that originate from the incomplete cancellation of virtual and real corrections. There seems to be no significant enhancement of these corrections at higher energies, where the NNLO QCD prediction for the partonic cross section becomes almost indistinguishable from the NLO QCD one. This suggests that QCD corrections to inclusive Higgs plus one-jet production will be milder at potential future 33 TeV and 100 TeV pp colliders. Since more phase space for harder gluon emission will be available, the threshold region will contribute a smaller fraction of the cross section at these higher-energy machines, reducing the effect of $\ln \beta$ terms. This is consistent with the pattern for inclusive Higgs production reported in Section 1.4.5. It would be interesting to study $\mathrm{d}\sigma_{\rm had}/\mathrm{d}\sqrt{s}$ at higher-energy pp machines upon completion of the full calculation.

We now discuss the resummation of jet-veto induced logarithms in exclusive jet bins. This has been the subject of intense discussion during the 7 TeV and 8 TeV LHC runs, and results combining resummation and fixed-order are now available for the zero-jet [81, 82, 83, 84, 85, 86] and one-jet [87, 88] bins. The resummation of large logarithms significantly reduces the theoretical uncertainties for the signal cross sections, and has a moderate impact on their central values. Given the continued importance of analyses utilizing exclusive jet bins during the 14 TeV run of the LHC and it potential future higher-energy colliders, it is important to

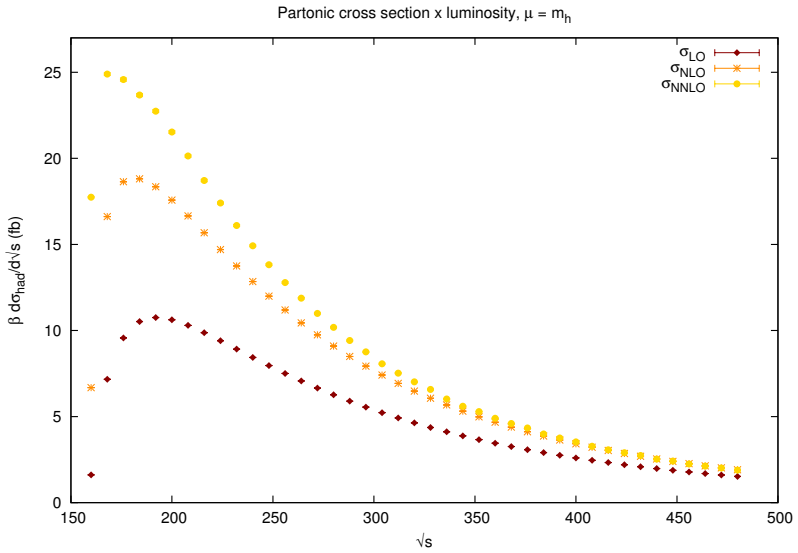

Figure 1-30. *Results for the product of partonic cross sections $gg \to H +$* jet *and parton luminosites in consecutive orders in perturbative QCD for an 8 TeV LHC at $\mu_R = \mu_F = m_h = 125$ GeV. The x-axis gives the value of partonic center-of-momemtum frame energy. See the text for further explanation.*

study how predictions scale with increasing collider energy. We consider first the exclusive Higgs plus one-jet bin in the gluon-fusion channel. The parametric form of the large logarithmic corrections is $\ln(\sqrt{s}/p_T^{cut})$, where $\sqrt{s}$ denotes the partonic center-of-momentum energy. As the collider energy increases, more events with large $\sqrt{s}$ contribute. We therefore expect the impact of the large logs and the resummation to increase at higher-energy machines, if the transverse momentum cut p_T^{cut} remains the same.

Shown below in Table 1-9 are cross sections for the parameter choices $m_H = 125$ GeV, $|\eta_J| < 4.5$, and using MSTW 2008 PDFs [9]. A fixed transverse momentum cut $p_T^{cut} = 30$ GeV is assumed, and the central scale choice $\mu = m_H/2$ is chosen for the fixed order predictions. Uncertainties are computed as described in Ref. [88], where the central values for the resummation are also discussed. Also shown is the K-factor describing the change in the prediction as the resummation is added. Results are presented at the NLO in fixed-order perturbation theory, and at NLL$'$ + NLO in resummed perturbation theory (the order-counting of resummed perturbation theory used here is described in Ref. [89]). The usefulness of the resummation in decreasing the theoretical uncertainties is clear. The fixed-order uncertainties grow with collider energy, reaching nearly 100% at 100 TeV. In contrast, they remain between $20\% - 25\%$ when the resummation is implemented. In 14 TeV and 33 TeV pp collisions, its effect is to slightly decrease the central value of the prediction, by up to 5%. This behavior changes significantly at 100 TeV, where instead a nearly 30% increase in the cross section is found. This is likely caused by the fixed-order perturbative expansion entirely breaking down and heading to negative values for such a large hierarchy between the hard scale and p_T^{cut}. This is suggested by the large uncertainty present in the NLO result. Resummation cures this behavior, and leads to an increase in the cross section. However, it is likely that the minimum jet transverse momentum would have to be increased at future facilities, due to the increased energy deposited by the underlying soft physics. We model this by increasing the minimum jet transverse momentum to 60 GeV in 33 TeV collisions, and to 80 GeV in 100 TeV collisions. The results are shown in Table 1-10. The change in K-factor as the collider energy is increased is ameliorated; a less than 15% increase in the cross section is found at 100 TeV.

	14 TeV	33 TeV	100 TeV
NLO	$12.48^{+34\%}_{-46\%}$	$40.17^{+54\%}_{-41\%}$	$131.3^{+72\%}_{-98\%}$
NLL′ + NLO	$11.73^{+27\%}_{-27\%}$	$39.71^{+24\%}_{-24\%}$	$166.9^{+22\%}_{-22\%}$
$K_{(\mathrm{NLL'+NLO})\mathrm{NLO}}$	0.940	0.989	1.27

Table 1-9. *Cross section central values and uncertainties for the exclusive Higgs plus one-jet bin for a fixed transverse momentum cut $p_T^{cut} = 30$ GeV. The results are shown in picobarns.*

	14 TeV	33 TeV	100 TeV
NLO	$12.48^{+34\%}_{-46\%}$	$26.90^{+30\%}_{-39\%}$	$91.23^{+38\%}_{-46\%}$
NLL′ + NLO	$11.73^{+27\%}_{-27\%}$	$27.44^{+24\%}_{-24\%}$	$103.0^{+24\%}_{-24\%}$
$K_{(\mathrm{NLL'+NLO})\mathrm{NLO}}$	0.940	1.02	1.13

Table 1-10. *Cross section central values and uncertainties for the exclusive Higgs plus one-jet bin, for the following transverse momentum cuts: $p_T^{cut} = 30$ GeV at 14 TeV, $p_T^{cut} = 60$ GeV at 33 TeV, and $p_T^{cut} = 80$ GeV at 100 TeV . The results are shown in picobarns.*

We study next the cross section for Higgs production via gluon-fusion in the exclusive zero-jet bin. This cross section has been studied through NNLL′ + NNLO in resummed perturbation theory in Ref. [86]. A careful study of clustering contributions of the form $\ln \mathrm{R}$, where R denotes the anti-k_T jet-radius parameter, was also performed in this reference. Numerical results for the Higgs plus zero-jet cross section at the NNLL′+NNLO order are presented in Table 1-11 for pp collisions at 14, 33, and 100 TeV. Also shown is ϵ_0, the fraction of events which fall into the zero-jet bin. A fixed transverse momentum cut $p_T^{cut} = 30$ GeV is assumed. The most notable effect upon increasing collider energy is the significant reduction of the fraction of events in the zero-jet bin, from 60% at 14 TeV to 44% at 100 TeV. The range of Bjorken-x becomes larger as the collider energy is increased, leading to a larger probability for additional radiation and consequently reducing the number of zero-jet events. A small reduction of scale uncertainty is found when going from 14 TeV collisions to higher energies, similar to what was found for the one-jet cross section in Table 1-9.

	14 TeV	33 TeV	100 TeV
$\sigma_{\mathrm{NNLL'+NNLO}}$	$33.25^{+5.5\%}_{-5.5\%}$	$104.2^{+3.9\%}_{-3.9\%}$	$364.2^{+4.4\%}_{-4.4\%}$
$\epsilon_0^{\mathrm{NNLL'+NNLO}}$	$0.596^{+4.4\%}_{-4.4\%}$	$0.522^{+4.9\%}_{-4.9\%}$	$0.438^{+4.4\%}_{-4.4\%}$

Table 1-11. *Central values and uncertainties for the exclusive Higgs plus zero-jet bin cross section and zero-jet event fraction, for a fixed transverse momentum cut $p_T^{cut} = 30$ GeV. The results are shown in picobarns.*

1.5.2 WH production at NNLO

Sometimes it is experimentally necessary to require an exclusive final state, for example by restricting the number of jets allowed to be present. This is true for some current LHC analyses and will no doubt continue to be true for higher energies. This requirement of an exclusive final state can result in the presence of large logarithms due to the unbalancing of the cancellation between positive real emission terms and

negative virtual corrections, thus affecting the convergence and reliability of the perturbative series. As an example, consider searches for Higgs boson production in the associated mode (VH). While this has been the major Higgs boson search channel at the Tevatron, at the LHC it suffers from large backgrounds. A precise measurement in this channel (with the Higgs decaying into a $b\bar{b}$ pair) can still be very useful in the years following the Higgs boson discovery in order to understand the Higgs coupling to b-quarks. A relative reduction in the background at the LHC can be achieved by requiring the vector boson and the Higgs boson to be at large transverse momentum, with no additional jets present greater than some threshold. While the impact of higher order QCD corrections is mild for the inclusive measurement, such restrictions can greatly affect the size of the higher order corrections and thus the convergence of the perturbative series. In this context, the issue was first raised in the original exclusive NNLO calculation of WH production [29].

In this report we address the extent to which this issue is exacerbated in predictions for higher energy proton-proton colliders. For the following study the transverse momentum of the W boson is required to be greater than 200 GeV. The Higgs boson decays into a $b\bar{b}$ pair that is reconstructed as a "fat jet" using the Cambridge-Aachen algorithm with $R = 1.2$. This fat jet must also be at large transverse momentum, greater than 200 GeV. In addition to these cuts, any additional jets were required have transverse momenta below 40 GeV. The study was repeated at 14, 33 and 100 TeV, with the results shown in Figure 1-31 (left). The cross section is plotted as a function of the transverse momentum of the fat (Higgs) jet. As the center-of-mass energy increases, the effect of such stringent cuts increases. There are large negative corrections when going from LO to NLO, resulting in a NLO K-factor (NLO/LO) as low as 0.3 (for 100 TeV). The corrections from NLO to NNLO by comparison are modest, but the strong reduction from LO to NLO indicates that the fixed order prediction may be unreliable, and a resummed cross section is necessary to achieve a reliable prediction. As alternative scenarios at higher energies, Figure 1-31 (right) shows the effect of raising the jet threshold to 60 GeV (at 33 TeV) and 80 GeV (at 100 TeV). In these cases, the effect of allowing additional phase space results in a better-behaved perturbative series, and cross sections that behave order-by-order in a manner that is more similar to the pattern observed for a 40 GeV veto at 14 TeV.

ACKNOWLEDGEMENTS

J. Rojo is supported by a Marie Curie Intra–European Fellowship of the European Community's 7th Framework Programme under contract number PIEF-GA-2010-272515.

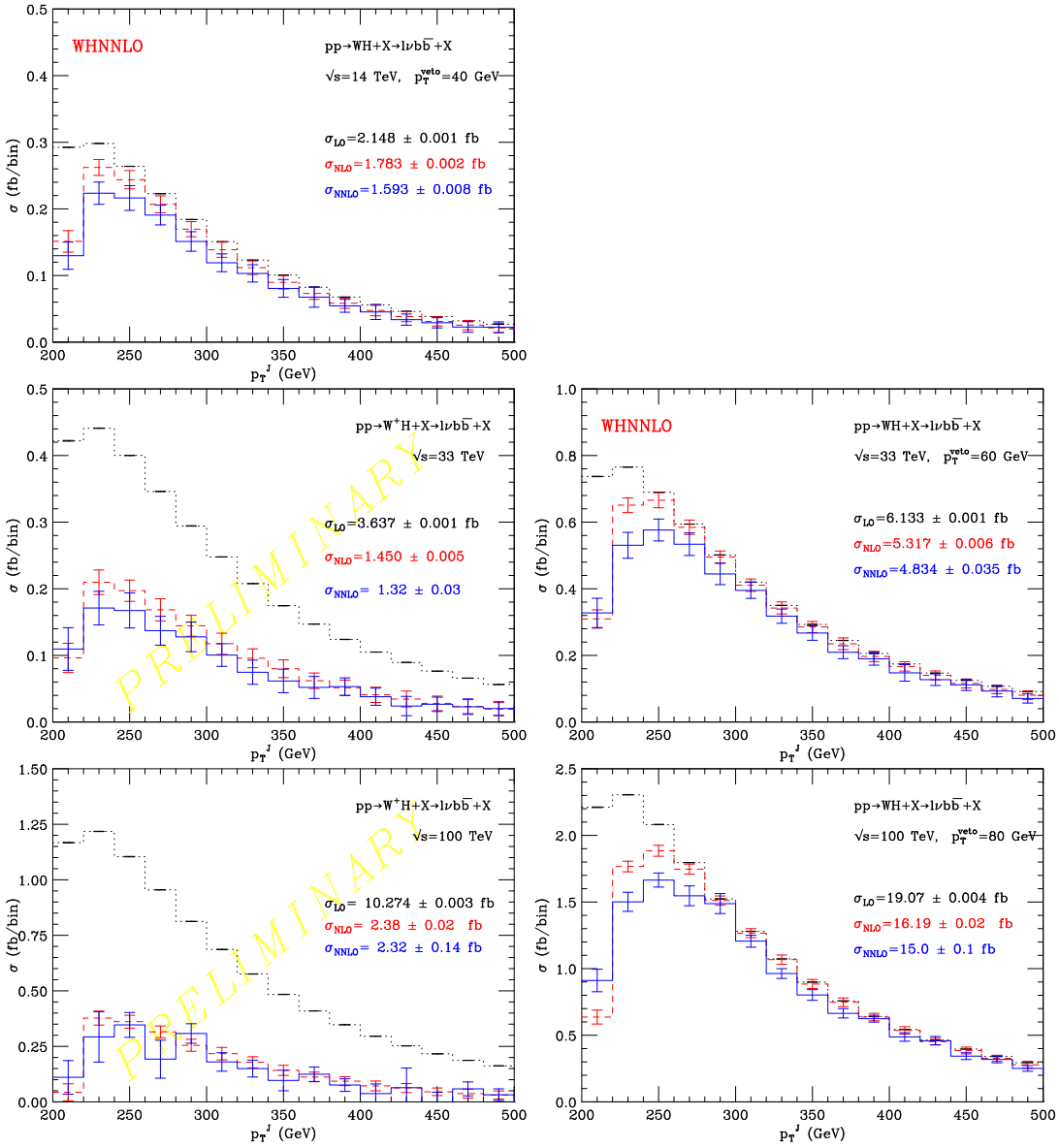

Figure 1-31. *The transverse momentum of the fat jet in WH production, at 14 TeV (top), 33 TeV (middle) and 100 TeV (bottom). In the left-hand column additional jets with transverse momenta above 40 GeV are vetoed, while in the right this veto is raised to 60 GeV at 33 TeV and 80 GeV at 100 TeV.*

References

[1] S. Forte and G. Watt, arXiv:1301.6754 [hep-ph].

[2] A. De Roeck and R. S. Thorne, Prog. Part. Nucl. Phys. **66**, 727 (2011) [arXiv:1103.0555 [hep-ph]].

[3] E. Perez and E. Rizvi, Rep. Prog. Phys. **76**, 046201 (2013) [arXiv:1208.1178 [hep-ex]].

[4] G. Bozzi, J. Rojo and A. Vicini, Phys. Rev. D **83**, 113008 (2011) [arXiv:1104.2056 [hep-ph]].

[5] S. Alekhin, J. Blumlein and S. Moch, Phys. Rev. D **86**, 054009 (2012) [arXiv:1202.2281 [hep-ph]].

[6] J. Gao, M. Guzzi, J. Huston, H. -L. Lai, Z. Li, P. Nadolsky, J. Pumplin and D. Stump *et al.*, arXiv:1302.6246 [hep-ph].

[7] V. Radescu [H1 and ZEUS Collaboration], PoS ICHEP **2010**, 168 (2010).

[8] A. M. Cooper-Sarkar [ZEUS and H1 Collaborations], PoS EPS **-HEP2011**, 320 (2011) [arXiv:1112.2107 [hep-ph]].

[9] A. D. Martin, W. J. Stirling, R. S. Thorne and G. Watt, Eur. Phys. J. C **63**, 189 (2009) [arXiv:0901.0002 [hep-ph]].

[10] R. D. Ball, V. Bertone, S. Carrazza, C. S. Deans, L. Del Debbio, S. Forte, A. Guffanti and N. P. Hartland *et al.*, Nucl. Phys. B **867**, 244 (2013) [arXiv:1207.1303 [hep-ph]].

[11] R. D. Ball, S. Carrazza, L. Del Debbio, S. Forte, J. Gao, N. Hartland, J. Huston and P. Nadolsky *et al.*, JHEP **1304**, 125 (2013) [arXiv:1211.5142 [hep-ph]].

[12] G. Aad *et al.* [ATLAS Collaboration], Phys. Rev. D **86**, 014022 (2012) [arXiv:1112.6297 [hep-ex]].

[13] S. Chatrchyan *et al.* [CMS Collaboration], Phys. Rev. D **87**, 112002 (2013) [arXiv:1212.6660 [hep-ex]].

[14] G. Aad *et al.* [ATLAS Collaboration], arXiv:1304.4739 [hep-ex].

[15] M. L. Mangano and J. Rojo, JHEP **1208**, 010 (2012) [arXiv:1206.3557 [hep-ph]].

[16] A. G. -D. Ridder, T. Gehrmann, E. W. N. Glover and J. Pires, Phys. Rev. Lett. **110**, 162003 (2013) [arXiv:1301.7310 [hep-ph]].

[17] M. Czakon, P. Fiedler and A. Mitov, arXiv:1303.6254 [hep-ph].

[18] M. Czakon, M. L. Mangano, A. Mitov and J. Rojo, arXiv:1303.7215 [hep-ph].

[19] R. D. Ball, V. Bertone, F. Cerutti, L. Del Debbio, S. Forte, A. Guffanti, J. I. Latorre and J. Rojo *et al.*, Nucl. Phys. B **849**, 296 (2011) [arXiv:1101.1300 [hep-ph]].

[20] R. D. Ball *et al.* [NNPDF Collaboration], Nucl. Phys. B **855**, 153 (2012) [arXiv:1107.2652 [hep-ph]].

[21] D. d'Enterria and J. Rojo, Nucl. Phys. B **860**, 311 (2012) [arXiv:1202.1762 [hep-ph]].

[22] L. Carminati, G. Costa, D. D'Enterria, I. Koletsou, G. Marchiori, J. Rojo, M. Stockton and F. Tartarelli, EPL **101**, 61002 (2013) [Europhys. Lett. **101**, 61002 (2013)] [arXiv:1212.5511 [hep-ph]].

[23] S. A. Malik and G. Watt, arXiv:1304.2424 [hep-ph].

[24] W. J. Stirling and E. Vryonidou, Phys. Rev. Lett. **109**, 082002 (2012) [arXiv:1203.6781 [hep-ph]].

[25] A. D. Martin, R. G. Roberts, W. J. Stirling and R. S. Thorne, Eur. Phys. J. C **39**, 155 (2005) [hep-ph/0411040].

[26] S. Carrazza, arXiv:1307.1131 [hep-ph].

[27] S. Carrazza, arXiv:1305.4179 [hep-ph].

[28] A. Bierweiler, T. Kasprzik, H. Kuhn and S. Uccirati, JHEP **1211**, 093 (2012) [arXiv:1208.3147 [hep-ph]].

[29] G. Ferrera, M. Grazzini and F. Tramontano, Phys. Rev. Lett. **107**, 152003 (2011) [arXiv:1107.1164 [hep-ph]].

[30] R. Boughezal, F. Caola, K. Melnikov, F. Petriello and M. Schulze, JHEP **1306**, 072 (2013) [arXiv:1302.6216 [hep-ph]].

[31] J. M. Campbell, R. K. Ellis and C. Williams, JHEP **1107**, 018 (2011) [arXiv:1105.0020 [hep-ph]].

[32] G. Aad *et al.* [ATLAS Collaboration], New J. Phys. **15**, 033038 (2013) [arXiv:1301.6872 [hep-ex]].

[33] R. D. Ball, M. Bonvini, S. Forte, S. Marzani and G. Ridolfi, Nucl. Phys. B **874**, 746 (2013) [arXiv:1303.3590 [hep-ph]].

[34] D. de Florian and M. Grazzini, Phys. Lett. B **718** (2012) 117 [arXiv:1206.4133 [hep-ph]].

[35] M. Bonvini, S. Forte and G. Ridolfi, Phys. Rev. Lett. **109**, 102002 (2012) [arXiv:1204.5473 [hep-ph]].

[36] S. Catani, D. de Florian, M. Grazzini and P. Nason, JHEP **0307** (2003) 028 [hep-ph/0306211].

[37] S. Buehler and A. Lazopoulos, arXiv:1306.2223 [hep-ph].

[38] N. Kidonakis and J. F. Owens, Phys. Rev. D **63**, 054019 (2001) [hep-ph/0007268].

[39] S. Frixione and B. R. Webber, JHEP **0206**, 029 (2002) [hep-ph/0204244].

[40] P. Nason, JHEP **0411**, 040 (2004) [hep-ph/0409146].

[41] S. Frixione, P. Nason and C. Oleari, JHEP **0711**, 070 (2007) [arXiv:0709.2092 [hep-ph]].

[42] S. Hoeche, F. Krauss, M. Schonherr and F. Siegert, JHEP **1304**, 027 (2013) [arXiv:1207.5030 [hep-ph]].

[43] R. Frederix and S. Frixione, JHEP **1212**, 061 (2012) [arXiv:1209.6215 [hep-ph]].

[44] S. Catani, F. Krauss, R. Kuhn and B. R. Webber, JHEP **0111**, 063 (2001) [hep-ph/0109231].

[45] L. Lonnblad, JHEP **0205**, 046 (2002) [hep-ph/0112284].

[46] M. L. Mangano, M. Moretti and R. Pittau, Nucl. Phys. B **632**, 343 (2002) [hep-ph/0108069].

[47] N. Lavesson and L. Lonnblad, JHEP **0812**, 070 (2008) [arXiv:0811.2912 [hep-ph]].

[48] L. Lnnblad and S. Prestel, JHEP **1303**, 166 (2013) [arXiv:1211.7278 [hep-ph]].

[49] S. Hoeche, F. Krauss, M. Schonherr and F. Siegert, Phys. Rev. Lett. **110**, 052001 (2013) [arXiv:1201.5882 [hep-ph]].

[50] S. Alioli, S. -O. Moch and P. Uwer, JHEP **1201**, 137 (2012) [arXiv:1110.5251 [hep-ph]].

[51] S. Hoeche, J. Huang, G. Luisoni, M. Schoenherr and J. Winter, arXiv:1306.2703 [hep-ph].

[52] Z. Nagy and D. E. Soper, JHEP **0709**, 114 (2007) [arXiv:0706.0017 [hep-ph]].

[53] S. Hoeche, F. Krauss, M. Schonherr and F. Siegert, JHEP **1209**, 049 (2012) [arXiv:1111.1220 [hep-ph]].

[54] S. Platzer and M. Sjodahl, JHEP **1207**, 042 (2012) [arXiv:1201.0260 [hep-ph]].

[55] S. Alioli, C. W. Bauer, C. J. Berggren, A. Hornig, F. J. Tackmann, C. K. Vermilion, J. R. Walsh and S. Zuberi, arXiv:1211.7049 [hep-ph].

[56] S. Alioli, C. W. Bauer, C. Berggren, A. Hornig, F. J. Tackmann, C. K. Vermilion, J. R. Walsh and S. Zuberi, arXiv:1305.5246 [hep-ph].

[57] J. R. Andersen and J. M. Smillie, JHEP **1001**, 039 (2010) [arXiv:0908.2786 [hep-ph]].

[58] J. R. Andersen and J. M. Smillie, JHEP **1106**, 010 (2011) [arXiv:1101.5394 [hep-ph]].

[59] J. R. Andersen, L. Lonnblad and J. M. Smillie, JHEP **1107**, 110 (2011) [arXiv:1104.1316 [hep-ph]].

[60] See web-page: `https://twiki.cern.ch/twiki/bin/view/LHCPhysics/HiggsEuropeanStrategy2012`.

[61] J. R. Andersen *et al.* [SM and NLO Multileg Working Group Collaboration], arXiv:1003.1241 [hep-ph].

[62] Z. Bern, L. J. Dixon, F. Febres Cordero, S. Hoeche, H. Ita, D. A. Kosower, D. Maitre and K. J. Ozeren, arXiv:1304.1253 [hep-ph].

[63] J. Beringer et al., Phys.Rev. D86 (2012) 010001; http://pdg.lbl.gov/ .

[64] G. Dissertori et al., "α_s from at an e+e- Z factory," Snowmass energy frontier Seatle meeting, July 2013.

[65] S. Schael *et al.* [ALEPH and DELPHI and L3 and OPAL and SLD and LEP Electroweak Working Group and SLD Electroweak Group and SLD Heavy Flavour Group Collaborations], Phys. Rept. **427**, 257 (2006) [hep-ex/0509008].

[66] S. Schael *et al.* [ALEPH and DELPHI and L3 and OPAL and LEP Electroweak Working Group Collaborations], arXiv:1302.3415 [hep-ex].

[67] P. A. Baikov, K. G. Chetyrkin and J. H. Kuhn, Phys. Rev. Lett. **101**, 012002 (2008) [arXiv:0801.1821 [hep-ph]].

[68] P. A. Baikov, K. G. Chetyrkin, J. H. Kuhn and J. Rittinger, Phys. Rev. Lett. **108**, 222003 (2012) [arXiv:1201.5804 [hep-ph]].

[69] P. Janot, M. Bachtis, and A. Blondel, "First Look at the Physics Case of TLEP," July 2013.

[70] CDF Collaboration, Phys. Rev. Lett. **88**, 042001 (2002) [hep-ex/0108034].

[71] D0 Collaboration, Phys. Rev. D **80** (2009) 111107.

[72] D0 Collaboration, Phys. Lett. B **718** (2012) 56.

[73] Eur. Phys. J. C **72** (2012) 2041.

[74] CMS Collaboration, CMS-PAS-QCD-11-003 (2012).

[75] CMS Collaboration, arXiv:1307.1907 [hep-ex].

[76] C. Anastasiou, R. Boughezal and F. Petriello, JHEP **0904**, 003 (2009) [arXiv:0811.3458 [hep-ph]].

[77] S. Dittmaier, A. Huss and C. Speckner, JHEP **1211**, 095 (2012) [arXiv:1210.0438 [hep-ph]].

[78] T. Becher and X. G. iTormo, arXiv:1305.4202 [hep-ph].

[79] G. Aad *et al.* [ATLAS Collaboration], Phys. Lett. B **716**, 62 (2012) [arXiv:1206.0756 [hep-ex]].

[80] S. Alioli, C. W. Bauer, C. J. Berggren, A. Hornig, F. J. Tackmann, C. K. Vermilion, J. R. Walsh and S. Zuberi, arXiv:1211.7049 [hep-ph].

[81] A. Banfi, G. P. Salam and G. Zanderighi, JHEP **1206**, 159 (2012) [arXiv:1203.5773 [hep-ph]].

[82] T. Becher and M. Neubert, JHEP **1207**, 108 (2012) [arXiv:1205.3806 [hep-ph]].

[83] F. J. Tackmann, J. R. Walsh and S. Zuberi, Phys. Rev. D **86**, 053011 (2012) [arXiv:1206.4312 [hep-ph]].

[84] A. Banfi, P. F. Monni, G. P. Salam and G. Zanderighi, Phys. Rev. Lett. **109**, 202001 (2012) [arXiv:1206.4998 [hep-ph]].

[85] T. Becher, M. Neubert and L. Rothen, arXiv:1307.0025 [hep-ph].

[86] I. W. Stewart, F. J. Tackmann, J. R. Walsh and S. Zuberi, arXiv:1307.1808 [hep-ph].

[87] X. Liu and F. Petriello, Phys. Rev. D **87**, 014018 (2013) [arXiv:1210.1906 [hep-ph]].

[88] X. Liu and F. Petriello, arXiv:1303.4405 [hep-ph].

[89] C. F. Berger, C. Marcantonini, I. W. Stewart, F. J. Tackmann and W. J. Waalewijn, JHEP **1104**, 092 (2011) [arXiv:1012.4480 [hep-ph]].

[90] J. H. Kuhn, A. Kulesza, S. Pozzorini and M. Schulze, Nucl. Phys. B **727**, 368 (2005) [hep-ph/0507178].

[91] J. H. Kuhn, A. Kulesza, S. Pozzorini and M. Schulze, Nucl. Phys. B **797**, 27 (2008) [arXiv:0708.0476 [hep-ph]].

[92] E. Maina, S. Moretti, M. R. Nolten and D. A. Ross, Phys. Lett. B **570**, 205 (2003) [hep-ph/0307021].

[93] E. Maina, S. Moretti and D. A. Ross, Phys. Lett. B **593**, 143 (2004) [Erratum-ibid. B **614**, 216 (2005)] [hep-ph/0403050].

[94] S. Moretti, M. R. Nolten and D. A. Ross, Nucl. Phys. B **759**, 50 (2006) [hep-ph/0606201].

[95] A. Denner, S. Dittmaier, T. Kasprzik and A. Muck, JHEP **0908**, 075 (2009) [arXiv:0906.1656 [hep-ph]].

[96] A. Denner, S. Dittmaier, T. Kasprzik and A. Muck, JHEP **1106**, 069 (2011) [arXiv:1103.0914 [hep-ph]].

[97] A. Denner, S. Dittmaier, T. Kasprzik and A. Mck, Eur. Phys. J. C **73**, 2297 (2013) [arXiv:1211.5078 [hep-ph]].

[98] S. Actis, A. Denner, L. Hofer, A. Scharf and S. Uccirati, JHEP **1304**, 037 (2013) [arXiv:1211.6316 [hep-ph]].

[99] P. Ciafaloni and D. Comelli, Phys. Lett. B **446**, 278 (1999) [hep-ph/9809321].

[100] M. Beccaria, P. Ciafaloni, D. Comelli, F. M. Renard and C. Verzegnassi, Phys. Rev. D **61**, 073005 (2000) [hep-ph/9906319].

[101] M. Ciafaloni, P. Ciafaloni and D. Comelli, Phys. Rev. Lett. **84**, 4810 (2000) [hep-ph/0001142].

[102] M. Ciafaloni, P. Ciafaloni and D. Comelli, Nucl. Phys. B **589**, 359 (2000) [hep-ph/0004071].

[103] M. Ciafaloni, P. Ciafaloni and D. Comelli, Phys. Rev. Lett. **87**, 211802 (2001) [hep-ph/0103315].

[104] A. Denner and S. Pozzorini, Eur. Phys. J. C **18**, 461 (2001) [hep-ph/0010201].

[105] A. Denner and S. Pozzorini, Eur. Phys. J. C **21**, 63 (2001) [hep-ph/0104127].

[106] J. H. Kuhn, A. Kulesza, S. Pozzorini and M. Schulze, Phys. Lett. B **609**, 277 (2005) [hep-ph/0408308].

[107] J. H. Kuhn, A. Kulesza, S. Pozzorini and M. Schulze, JHEP **0603**, 059 (2006) [hep-ph/0508253].

[108] J. H. Kuhn, A. Kulesza, S. Pozzorini and M. Schulze, Phys. Lett. B **651**, 160 (2007) [hep-ph/0703283 [HEP-PH]].

[109] E. Accomando, A. Denner and S. Pozzorini, JHEP **0703**, 078 (2007) [hep-ph/0611289].

[110] M. Chiesa, G. Montagna, L. Barze', M. Moretti, O. Nicrosini, F. Piccinini and F. Tramontano, arXiv:1305.6837 [hep-ph].

[111] M. L. Mangano, M. Moretti, F. Piccinini, R. Pittau and A. D. Polosa, JHEP **0307**, 001 (2003) [hep-ph/0206293].

[112] G. Aad *et al.* [ATLAS Collaboration], Phys. Lett. B **710**, 67 (2012) [arXiv:1109.6572 [hep-ex]].

[113] S. Chatrchyan *et al.* [CMS Collaboration], JHEP **1108**, 155 (2011) [arXiv:1106.4503 [hep-ex]].

[114] K. Melnikov and F. Petriello, Phys. Rev. D **74**, 114017 (2006) [hep-ph/0609070].

[115] R. Gavin, Y. Li, F. Petriello and S. Quackenbush, Comput. Phys. Commun. **182**, 2388 (2011) [arXiv:1011.3540 [hep-ph]].

[116] Y. Li and F. Petriello, Phys. Rev. D **86**, 094034 (2012) [arXiv:1208.5967 [hep-ph]].

[117] V. V. Sudakov, Sov. Phys. JETP **3** (1956) 65.

[118] V. S. Fadin, L. N. Lipatov, A. D. Martin and M. Melles, Phys. Rev. D **61**, 094002 (2000) [hep-ph/9910338].

[119] U. Baur, Phys. Rev. D **75** (2007) 013005 [hep-ph/0611241].

[120] J. L. Abelleira Fernandez *et al.* [LHeC Study Group], J.Phys.G. **39** (2012) 075001.

[121] J. L. Abelleira Fernandez *et al.* [LHeC Study Group], arXiv:1211.5102, unpublished.

[122] O. Brüning and M. Klein, Mod. Phys. Lett. A **28** (2013) 16, 1330011 [arXiv:1305.2090].

[123] G. Azuelos *et al.*, "New Physics with the LHeC", Poster submitted to EPS, Stockholm, July 2013.

[124] F. D. Aaron *et al.* [H1 and ZEUS Collaboration], JHEP **1001** (2010) 109 [arXiv:0911.0884].

[125] F. D. Aaron *et al.* [H1 Collaboration], Eur. Phys. J. C **64**, 561 (2009) [arXiv:0904.3513].

[126] F. James and M. Roos, Comput. Phys. Commun. **10**, 343 (1975).

[127] S. Bethke *et al.*, "Workshop on Precision Measurements of α_s," arXiv:1110.0016.

[128] S. Alekhin, J. Blümlein and S. Moch, Phys. Rev. D **86** (2012) 054009 and arXiv:1303.1073.

[129] G. Aad *et al.* [ATLAS Collaboration], Phys. Rev. D **85**, 092002 (2012) [arXiv:1201.1276 [hep-ex]].

[130] G. Aad *et al.* [ATLAS Collaboration], Phys. Rev. D **85**, 032009 (2012) [arXiv:1111.2690 [hep-ex]].

[131] C. F. Berger, Z. Bern, L. J. Dixon, F. Febres Cordero, D. Forde, T. Gleisberg, H. Ita and D. A. Kosower *et al.*, Phys. Rev. Lett. **106**, 092001 (2011) [arXiv:1009.2338 [hep-ph]].

[132] S. Chatrchyan *et al.* [CMS Collaboration], Phys. Lett. B **710**, 91 (2012) [arXiv:1202.1489 [hep-ex]].

[133] S. Chatrchyan *et al.* [CMS Collaboration], Phys. Rev. Lett. **109**, 171803 (2012) [arXiv:1207.1898 [hep-ex]].

[134] S. Chatrchyan *et al.* [CMS Collaboration], JHEP **1201**, 010 (2012) [arXiv:1110.3226 [hep-ex]].

[135] S. Chatrchyan *et al.* [CMS Collaboration], JHEP **1206**, 126 (2012) [arXiv:1204.1643 [hep-ex]].

[136] ATLAS Collaboration, http://cds.cern.ch/record/1562879 (2013).

[137] CMS Collaboration, http://cds.cern.ch/record/1546778 (2013).

[138] CMS Collaboration, http://cds.cern.ch/record/1522476 (2013).

[139] CMS Collaboration, https://cdsweb.cern.ch/record/1537320 (2013).

[140] CMS Collaboration, https://cdsweb.cern.ch/record/1547589 (2013).

[141] ATLAS Collaboration, http://cds.cern.ch/record/1525524 (2013).

[142] ATLAS Collaboration, http://cds.cern.ch/record/1557773 (2013).